Role of the transcriptional regulator SP140 in resistance to bacterial infections via repression of type I interferons

Daisy X. Ji[1*], Kristen C. Witt[1*], Dmitri I. Kotov[1,2], Shally R. Margolis[1], Alexander Louie[1], Victoria Chevée[1], Katherine J. Chen[1,2], Moritz Gaidt[1,2], Harmandeep S. Dhaliwal[3], Angus Y. Lee[3], Stephen Nishimura[4], Dario S. Zamboni[5], Igor Kramnik[6], Daniel A. Portnoy[1,7,8], K. Heran Darwin[9], Russell E. Vance[1,2,3**]

[1] Division of Immunology and Pathogenesis, Department of Molecular and Cell Biology, University of California, Berkeley, CA 94720 USA

[2] Howard Hughes Medical Institute, University of California, Berkeley, CA 94720 USA

[3] Cancer Research Laboratory, University of California, Berkeley, CA 94720 USA

[4] Department of Pathology, University of California, San Francisco, CA 94143 USA

[5] Department of Cell Biology, Ribeirão Preto Medical School, University of São Paulo, Ribeirão Preto, São Paulo, Brazil.

[6] The National Emerging Infectious Diseases Laboratory, Department of Medicine (Pulmonary Center), and Department of Microbiology, Boston University School of Medicine, Boston, MA 02118 USA.

[7] Division of Biochemistry, Biophysics and Structural Biology, Department of Molecular and Cell Biology, University of California, Berkeley, CA 94720 USA

[8] Department of Plant and Microbial Biology, University of California, Berkeley, CA 94720 USA

[9] Department of Microbiology, New York University Grossman School of Medicine, New York, NY, USA

* These authors contributed equally to this work.

** e-mail: rvance@berkeley.edu

Impact Statement: Repression of type I interferons by SP140 is essential for resistance to *Legionella pneumophila* and *Mycobacterium tuberculosis*.

Abstract

Type I interferons (IFNs) are essential for anti-viral immunity, but often impair protective immune responses during bacterial infections. An important question is how type I IFNs are strongly induced during viral infections, and yet are appropriately restrained during bacterial infections. The *Super susceptibility to tuberculosis 1* (*Sst1*) locus in mice confers resistance to diverse bacterial infections. Here we provide evidence that *Sp140* is a gene encoded within the *Sst1* locus that represses type I IFN transcription during bacterial infections. We generated *Sp140*$^{-/-}$ mice and find they are susceptible to infection by *Legionella pneumophila* and *Mycobacterium tuberculosis*. Susceptibility of *Sp140*$^{-/-}$ mice to bacterial infection was rescued by crosses to mice lacking the type I IFN receptor (*Ifnar*$^{-/-}$). Our results implicate *Sp140* as an important negative regulator of type I IFNs that is essential for resistance to bacterial infections.

42 **Introduction**

43 Type I interferons (IFNs) comprise a group of cytokines, including interferon-β and multiple
44 interferon-α isoforms, that are essential for immune defense against most viruses (Stetson &
45 Medzhitov, 2006). Type I IFNs signal through a cell surface receptor, the interferon alpha and
46 beta receptor (IFNAR), to induce an 'anti-viral state' that is characterized by the transcriptional
47 induction of hundreds of interferon stimulated genes (ISGs) (Schneider et al., 2014). Many ISGs
48 encode proteins with direct anti-viral activities. Type I IFNs also promote anti-viral responses by
49 cytotoxic T cells and Natural Killer cells. Accordingly, *Ifnar*$^{-/-}$ mice are highly susceptible to
50 most viral infections.

51 Many ISGs are also induced by IFN-γ (also called type II IFN). However, type I and type
52 II IFNs appear to be specialized for the control of different classes of pathogens (Crisler & Lenz,
53 2018). Whereas type I IFNs are predominantly anti-viral, the ISGs induced by IFN-γ appears to
54 be especially important for the control of diverse intracellular pathogens, including parasites and
55 bacteria. In contrast, type I IFNs play complex roles during bacterial infections (Boxx & Cheng,
56 2016; Donovan et al., 2017; McNab et al., 2015; Moreira-Teixeira et al., 2018). Some ISGs
57 induced by type I IFN, most notably certain guanylate binding proteins (GBPs), have anti-
58 bacterial activities (Pilla-Moffett et al., 2016). At the same time, other proteins induced by type I
59 IFNs, including interleukin-10 (IL-10) and IL-1 receptor antagonist (IL-1RA), impair anti-
60 bacterial immunity (Boxx & Cheng, 2016; Ji et al., 2019; Mayer-Barber et al., 2014). As a result,
61 the net effect of type I IFN is often to increase susceptibility to bacterial infections. For example,
62 *Ifnar*$^{-/-}$ mice exhibit enhanced resistance to *Listeria monocytogenes* (Auerbuch et al., 2004;
63 Carrero et al., 2004; O'Connell et al., 2004) and *Mycobacterium tuberculosis* (Donovan et al.,
64 2017; Dorhoi et al., 2014; Ji et al., 2019; Mayer-Barber et al., 2014; Moreira-Teixeira et al.,
65 2018). Multiple mechanisms appear to explain resistance of *Ifnar*$^{-/-}$ mice to *L. monocytogenes*,
66 including a negative effect of type I IFNs on protective IFN-γ signaling (Rayamajhi et al., 2010).
67 Likewise, diverse mechanisms underlie the negative effects of type I IFNs during *M.*
68 *tuberculosis* infection, including alterations of eicosanoid production (Mayer-Barber et al., 2014)
69 and the induction of IL-1Ra (Ji et al., 2019), both of which impair protective IL-1 responses.

70 As an experimental model for dissecting the mechanisms by which inappropriate type I
71 IFN responses are restrained during bacterial infections, we have compared mice harboring
72 different haplotypes of the *Super susceptibility to tuberculosis 1* (*Sst1*) locus (Pan et al., 2005;
73 Pichugin et al., 2009). The *Sst1* locus encompasses about 10M base pairs of mouse chromosome
74 1, a region that contains approximately 50 genes. Mice harboring the susceptible (S) haplotype of
75 *Sst1*, derived from the C3H/HeBFeJ mouse strain, succumb relatively rapidly to *M. tuberculosis*
76 infection as compared to isogenic mice harboring the resistant (R) *Sst1* haplotype (derived from

77 C57BL/6 mice). Likewise, *Sst1*^{S} mice also exhibit enhanced susceptibility to *Listeria*
78 *monocytogenes* (Boyartchuk et al., 2004; Pan et al., 2005) and *Chlamydia pneumoniae* (He et al.,
79 2013). The susceptibility of *Sst1*^{S} mice to *M. tuberculosis* was reversed by crossing to *Ifnar*$^{-/-}$
80 mice (He et al., 2013; Ji et al., 2019), thereby demonstrating the causative role of type I IFNs in
81 driving the susceptibility phenotype. Although multiple type I IFN-induced genes are likely
82 responsible for the detrimental effects of type I IFNs during bacterial infections, heterozygous
83 deficiency of a single type I IFN-induced gene, *Il1rn* (encoding IL-1 receptor antagonist), was
84 sufficient to almost entirely reverse the susceptibility of *Sst1*^{S} mice to *M. tuberculosis* (Ji et al.,
85 2019).

86 The *Sst1*^{R} haplotype is dominant over the *Sst1*^{S} haplotype, suggesting that *Sst1*^{R} likely
87 encodes a protective factor that is absent from *Sst1*^{S} mice (Pan et al., 2005; Pichugin et al., 2009).
88 By comparing gene expression in *Sst1*^{R} versus *Sst1*^{S} mice, *Sp110* (also known as *Ipr1*) was
89 discovered as an *Sst1*-encoded gene that is transcribed selectively in *Sst1*^{R} mice (Pan et al.,
90 2005). Transgenic expression of *Sp110* in *Sst1*^{S} mice partially restored resistance to *M.*
91 *tuberculosis* and *L. monocytogenes* (Pan et al., 2005). However, the causative role of *Sp110* in
92 conferring resistance to bacterial infections was not confirmed by the generation of *Sp110*-
93 deficient B6 mice. Null mutations of human *SP110* are associated with VODI (hepatic veno-
94 occlusive disease with immunodeficiency syndrome, OMIM 235550), but not mycobacterial
95 diseases (Roscioli et al., 2006). Some studies have found polymorphisms in *SP110* to be
96 associated with susceptibility to TB, though not consistently so across different ethnic groups
97 (Chang et al., 2018; Fox et al., 2014; Lei et al., 2012; Png et al., 2012; Thye et al., 2006; Tosh et
98 al., 2006; Zhang et al., 2017).

99 In humans and mice, SP110 is a part of the Speckled Protein (SP) family of nuclear
100 proteins, consisting of SP100, SP110 and SP140 (and SP140L in humans only) (Fraschilla &
101 Jeffrey, 2020). The SP family members also exhibit a high degree of similarity to AIRE, a
102 transcriptional regulator that promotes tolerance to self-antigens by inducing their expression in
103 thymic epithelial cells (Anderson & Su, 2016; Fraschilla & Jeffrey, 2020; Perniola & Musco,
104 2014). All members of the SP-AIRE family in both mice and humans have an N-terminal SP100
105 domain that appears to function as a homotypic protein-protein interaction domain (Fraschilla &
106 Jeffrey, 2020; Huoh et al., 2020). The SP100 domain is closely related to the Caspase Activation
107 and Recruitment Domain (CARD), though SP family members are not believed to activate
108 caspases. SP-AIRE proteins also contain a DNA-binding SAND domain (Bottomley et al.,
109 2001). Certain SP isoforms, including all human full-length SP family members and mouse
110 SP140, also include a plant homeobox domain (PHD) and a bromodomain (BRD) (Fraschilla &
111 Jeffrey, 2020). The genes encoding SP family proteins are linked in a small cluster in both mouse

112 and human genomes and are inducible by IFN-γ in a variety of cell lines. The mouse
113 *Sp100/110/140* gene cluster is adjacent to a highly repetitive 'homogenously staining region'
114 (HSR) of chromosome 1 that remains poorly assembled in the most recent genome assembly due
115 to the presence of as many as 40 near-identical repeats of *Sp110*-like sequences (Pan et al., 2005;
116 Weichenhan et al., 2001). Most of these repeated *Sp110*-like sequences in the HSR appear to be
117 either incomplete copies of *Sp110* or pseudogenes that are not believed to be translated, but their
118 presence has nevertheless complicated genetic targeting and analysis of the SP gene family.

119 With the advent of CRISPR–Cas9-based methods (Wang et al., 2013), we were able to
120 generate *Sp110*$^{-/-}$ mice on the B6 background. Surprisingly, we found that *Sp110*$^{-/-}$ mice do not
121 phenocopy the susceptibility of *Sst1*^{S} mice to *M. tuberculosis* infection *in vivo*. Upon analysis of
122 additional candidate genes in the *Sst1* locus, we found that B6.*Sst1*^{S} mice also lack expression of
123 *Sp140*. To test whether loss of *Sp140* might account for the susceptibility of *Sst1*^{S} mice to
124 bacterial infections, we generated *Sp140*$^{-/-}$ mice. We found these mice are as susceptible as
125 B6.*Sst1*^{S} mice to the intracellular bacterial pathogens *M. tuberculosis* and *Legionella*
126 *pneumophila*. Similar to B6.*Sst1*^{S} mice, *Sp140*$^{-/-}$ mice exhibit an exacerbated type I IFN
127 response after bacterial infection, and the susceptibility of *Sp140*$^{-/-}$ mice is rescued by crosses to
128 *Ifnar*$^{-/-}$ mice. Our results suggest that loss of *Sp140* explains the susceptibility to bacterial
129 infections associated with the *Sst1*^{S} haplotype. These data further suggest that SP140 is a novel
130 negative regulator of type I IFN responses that is essential for protection against intracellular
131 bacterial infections.

132

133 **Results**

134 ***Sp110*$^{-/-}$ mice are not susceptible to *M. tuberculosis.*** Loss of *Sp110* expression was proposed to
135 account for the susceptibility of mice carrying the *Sst1*^{S} haplotype to bacterial infections (Pan et
136 al., 2005). We first confirmed that bone marrow-derived macrophages (BMMs) from B6.*Sst1*^{S}
137 mice lack expression of *Sp110* protein (Figure 1A). To determine whether loss of *Sp110* confers
138 susceptibility to bacterial infections, we used CRISPR–Cas9 to target exon 3 of *Sp110* to
139 generate *Sp110*$^{-/-}$ mice on the C57BL/6 (B6) background (Figure 1– figure supplement 1). We
140 generated three independent *Sp110*$^{-/-}$ lines, denoted as lines 61, 65 and 71 (Figure 1A, Figure 1–
141 figure supplement 1). All three lines lacked expression of *Sp110*, as verified using three different
142 antibodies (Figure 1A). *Sp110*$^{-/-}$ mice are viable and are born at normal Mendelian ratios and
143 litter sizes. When aerosol infected with a low-dose of *M. tuberculosis*, *Sp110*$^{-/-}$ mice did not
144 phenocopy the susceptibility observed in B6.*Sst1*^{S} mice (Figure 1B-D). At day 25 post-infection,
145 *Sp110*$^{-/-}$ lungs resembled those of wild-type B6 mice (Figure 1B), and harbored fewer bacteria

146 than the lungs of B6.*Sst1*^{S} mice, similar to both the B6 and *Sp110*$^{+/-}$ littermates (Figure 1C).
147 Likewise, the survival of infected *Sp110*$^{-/-}$ mice was indistinguishable from B6 mice, and mice
148 of both genotypes survived considerably longer than the B6.*Sst1*^{S} mice (Figure 1D). Thus,
149 despite the absence of *Sp110* from *Sst1*^{S} mice, our results indicate that the loss of *Sp110* is not
150 sufficient to replicate the susceptibility to *M. tuberculosis* associated with the *Sst1*^{S} locus.

151 ***Sp140*$^{-/-}$ mice are susceptible to bacterial infections.** Given that *Sp110* deficiency did not
152 phenocopy the susceptibility of *Sst1*^{S} mice, we asked whether any other genes found within the
153 *Sst1* locus differ in expression between B6 and B6.*Sst1*^{S} BMMs. We noted that a homolog of
154 *Sp110* called *Sp140* was also reduced in expression in B6.*Sst1*^{S} cells compared to B6 cells
155 (Figure 2A). Immunoblot confirmed that IFN-γ treated BMMs from B6.*Sst1*^{S} mice do not
156 produce SP140 protein (Figure 2B). We therefore used CRISPR–Cas9 to generate two
157 independent lines of *Sp140*$^{-/-}$ mice on a pure B6 background (Figure 2 – figure supplement 1A-
158 C). Our analysis focused primarily on line 1, which we found lacked expression of SP140
159 protein (Figure 2B) but retains the production of SP110 protein (Figure 2 – figure supplement
160 1D). Like *Sp110*$^{-/-}$ and *Sst1*^{S} mice, *Sp140*$^{-/-}$ mice are viable, fertile and born at the expected
161 Mendelian ratios. When infected with *M. tuberculosis*, however, *Sp140*$^{-/-}$ mice exhibited high
162 bacterial burdens in their lungs, similar to B6.*Sst1*^{S} mice and significantly greater than B6,
163 *Sp110*$^{-/-}$ or *Sp140*$^{+/-}$ littermate mice at day 28 post-infection (Figure 2C, Figure 2 – figure
164 supplement 1E).
165 We performed hematoxylin and eosin (H&E) staining of lung sections from B6, *Sp140*$^{-/-}$,
166 *Sp110*$^{-/-}$, and B6.*Sst1*^{S} mice 25 days after *M. tuberculosis* infection, and qualitatively assessed
167 macrophage, lymphoid, and granulocyte infiltration as well as the extent of necrosis (Figure 2D,
168 Figure 2 – figure supplement 2). We found that *Sp140*$^{-/-}$ and B6.*Sst1*^{S} lungs showed moderately
169 increased granulocyte infiltration by 25 days post infection, with apparently more severe
170 infiltration in *Sp140*$^{-/-}$ mice than in B6.*Sst1*^{S} mice, though this difference is not statistically
171 significant. We could also discern some areas of necrosis in the *Sp140*$^{-/-}$ lungs, although our
172 samples were taken at an early timepoint that precedes the formation of hypoxic lesions observed
173 in B6.*Sst1*^{S} lungs upon *M. tuberculosis* infection (Harper et al., 2012). The increased
174 susceptibility of *Sp140*$^{-/-}$ mice was accompanied by significant weight loss and shortened
175 survival upon infection with *M. tuberculosis*, again phenocopying the B6.*Sst1*^{S} mice (Figure 2E-
176 F). Both of the independent lines of *Sp140*$^{-/-}$ mice were similarly susceptible to *M. tuberculosis*
177 (Figure 2 – figure supplement 1E). We also found that both B6.*Sst1*^{S} and *Sp140*$^{-/-}$ mice were
178 more susceptible to the intracellular Gram-negative bacterium *Legionella pneumophila*, as
179 compared to the B6 and *Sp110*$^{-/-}$ mice (Figure 2G).
180 An important caveat to the use of CRIPSR–Cas9 to generate *Sp140*$^{-/-}$ mice is the

181 presence of an unknown number of nearly identical *Sp140*-like genes in the *Sst1* locus and non-
182 localized chromosome 1 genome contigs (that presumably map to the adjacent HSR that remains
183 unassembled by the mouse genome project). It is possible that the guide RNA we used to disrupt
184 exon 3 of *Sp140* also disrupted these uncharacterized *Sp140*-like genes, though it is not clear if
185 these uncharacterized *Sp140*-like genes give rise to functional proteins. Nevertheless, to identify
186 potential mutated off-target genes in our *Sp140*$^{-/-}$ mice, we amplified exons 2/3 of *Sp140* and
187 any potential paralogs from genomic DNA and from cDNA derived from *M. tuberculosis*-
188 infected lungs, and subjected the amplicons to deep sequencing (Figure 2 – figure supplement 3).
189 Although we found evidence for several edited *Sp140*-like exons in our *Sp140*$^{-/-}$ mice, only one
190 of these edited off-target genes was found to be detectably expressed from analysis of RNA-seq
191 data from *M. tuberculosis*-infected lungs, and this off-target appeared to be edited in only one of
192 our founder lines (Figure 2 – figure supplement 3B). Thus, mutation of *Sp140* itself is the most
193 parsimonious explanation for susceptibility of our *Sp140*$^{-/-}$ mice, a conclusion further supported
194 by complementation of the mutation in BMMs (see below, Figure 2 – figure supplement 4).
195 Collectively our results strongly suggest that the lack of expression of *Sp140* in B6.*Sst1*^{S} mice
196 explains the broad susceptibility of these mice to bacterial infections.

197 **Enhanced type I IFN responses in *Sp140*$^{-/-}$ and B6.*Sst1*^{S} mice.** We and others previously
198 reported that TNFα induces higher levels of type I IFN-induced genes in *Sst1*^{S} BMMs as
199 compared to B6 BMMs (Bhattacharya et al., 2021; Ji et al., 2019). We also observed higher
200 levels of *Ifnb* transcripts in the lungs of B6.*Sst1*^{S} mice infected with *M. tuberculosis*, as
201 compared to infected B6 mice (Ji et al., 2019). Similar to B6.*Sst1*^{S} BMMs, *Sp140*$^{-/-}$ BMMs also
202 exhibited elevated expression of *Ifnb* and interferon-stimulated genes (ISGs) when stimulated
203 with TNFα (Figure 2 – figure supplement 4A). Importantly, we were also able to complement
204 the enhanced IFN phenotype of *Sp140*$^{-/-}$ BMMs by transducing *Sp140*$^{-/-}$ BMMs with a
205 retrovirus expressing a *Sp140* cDNA driven by a minimal CMV promoter (Figure 2 – figure
206 supplement 4B). Repression of *Ifnb* by overexpression of *Sp140* in *Sp140*$^{-/-}$ BMMs was
207 selective, as *Sp140* overexpression did not repress the transcription of *Tnfa* induced by TNFα
208 (Figure 2 – figure supplement 4B).

209 In addition to enhanced type I IFN responses to TNFα, we also observed that both
210 B6.*Sst1*^{S} and *Sp140*$^{-/-}$ BMMs show increased cell death *in vitro* upon stimulation with polyI:C
211 compared to B6 BMMs, as measured by lactate dehydrogenase (LDH) release (Figure 3 – figure
212 supplement 1). This result is analogous to previous findings that B6.*Sst1*^{S} BMMs die upon
213 sustained TNF stimulation (Brownhill et al., 2020). The enhanced polyI:C-induced LDH release
214 in both *Sp140*$^{-/-}$ and B6.*Sst1*^{S} BMMs was blunted upon genetic deletion of *Ifnar* (Figure 3 –

215 figure supplement 1), consistent with type I IFNs playing an important role in the cell death
216 phenotype.
217 When infected with *M. tuberculosis*, the lungs of *Sp140*$^{-/-}$ and B6.*Sst1*^{S} mice also
218 exhibited higher levels of *Ifnb* transcript as compared to B6, *Sp110*$^{-/-}$ and *Sp140*$^{+/-}$ littermate
219 mice (Figure 3A). The lungs of *Sp140*$^{-/-}$ exhibited moderately increased levels of *Ifnb* transcript
220 compared to B6.*Sst1*^{S} during *M. tuberculosis* infection, which could be a result of partial low
221 expression of *Sp140* in B6.*Sst1*^{S} mice, or possibly microbiota differences between the strains.
222 Since we do not observe significant differences in weight, survival, or CFU between *Sp140*$^{-/-}$
223 and B6.*Sst1*^{S} mice upon *M. tuberculosis* infection, there is no evidence that modest differences in
224 type I IFN responses are of functional significance. We also found that during *L. pneumophila*
225 infection, *Sp140*$^{-/-}$ mice expressed more *Ifnb* in their lungs, as compared to B6 mice (Figure 3B).
226 Importantly, elevated *Ifnb* was evident at 48 hours post-infection when there is no difference in
227 bacterial burdens between the genotypes, and at 96 hours post-infection, when *Sp140*$^{-/-}$ mice
228 have greater bacterial burdens (Figure 3B).

229 **Infected *Sp140*$^{-/-}$ and B6.*Sst1*^{S} lungs show similar gene expression patterns.** We used RNA
230 sequencing to analyze the global gene expression patterns in *M. tuberculosis*-infected lungs of
231 B6, *Sp110*$^{-/-}$, *Sp140*$^{-/-}$ and B6.*Sst1*^{S} mice at day 28 post-infection (Figure 4). Principal
232 component analysis revealed that while there is spread among individual samples, the expression
233 pattern of *Sp140*$^{-/-}$ and B6.*Sst1*^{S} lungs segregates from the expression pattern in B6 and *Sp110*$^{-/-}$
234 lungs along the PC1 axis (77% of variance) (Figure 4A). Notably, the *Sp140*$^{-/-}$ and B6.*Sst1*^{S} only
235 separated along the PC2 axis, which accounts for only 9% of the variance in our RNA-seq data.
236 Euclidean distance analysis revealed a similar pattern, with B6.*Sst1*^{S} and *Sp140*$^{-/-}$ mice
237 clustering together, and away from B6 and *Sp110*$^{-/-}$ mice (Figure 4B). At the time point
238 analyzed (28 dpi), both *Sp140*$^{-/-}$ and B6.*Sst1*^{S} mice exhibit higher bacterial burdens than B6 and
239 *Sp110*$^{-/-}$ mice (Figure 2C). Thus, the similarity of the gene expression profile of B6.*Sst1*^{S} and
240 *Sp140*$^{-/-}$ lungs may merely reflect increased inflammation in these lungs. Alternatively, the
241 increased bacterial burdens may be due to a similarly enhanced type I IFN response in these
242 mice, which leads to secondary bacterial outgrowth and inflammation. Therefore, we specifically
243 compared the change in expression of two subsets of genes: (1) hallmark inflammatory response
244 pathway (Figure 4C) and (2) type I interferon response genes (Figure 4D). This analysis revealed
245 that B6.*Sst1*^{S} and *Sp140*$^{-/-}$ mice not only show a similarly increased inflammatory gene
246 signature, as expected, but in addition showed a similarly increased type I IFN gene signature.
247 We validated the elevated expression of the interferon stimulated gene *Il1rn* in both B6.*Sst1*^{S} and
248 *Sp140*$^{-/-}$ mice during *M. tuberculosis* infection by RT-qPCR (Figure 4 – figure supplement 1).
249 The expression of *Sp110* and the SP family member *Sp100* in *Sp140*$^{-/-}$ mice during *M*

250 *tuberculosis* infection was unimpaired compared to B6, and the expression level of *Sp100* was
251 unchanged between *Sp140*$^{-/-}$ and B6.*Sst1*^{S} mice (Figure 4 – figure supplement 2). We also did
252 not observe major changes in expression (>2-fold change) of *Sp100* or *Sp140* in *Sp110*$^{-/-}$ mice
253 during *M tuberculosis* infection (Figure 4 – figure supplement 2). Overall, the expression of
254 additional SP family members in *Sp140*$^{-/-}$ and *Sp110*$^{-/-}$ mice is intact, which suggests that the
255 targeting of these genes had specific rather than unanticipated epistatic effects. Therefore,
256 deficiency in *Sp140* is likely the primary driver of susceptibility in *Sp140*$^{-/-}$ mice, while the
257 resistance of *Sp110*$^{-/-}$ mice likely derives from normal expression of *Sp140* rather than aberrant
258 changes in the expression of other SP family members.

259 Only 269 genes were significantly differentially expressed (adjusted p-value <0.05)
260 between *Sp140*$^{-/-}$ and B6.*Sst1*^{S} samples, whereas 1520 genes were significantly differentially
261 expressed between *Sp140*$^{-/-}$ and B6. Within the 269 genes differentially expressed between
262 *Sp140*$^{-/-}$ and B6.*Sst1*^{S}, 62 were immunoglobulin genes and 62 were annotated as pseudogenes
263 and most differences are only of modest significance (Figure 4E). The differentially expressed
264 genes are not linked to the *Sst1*^{S} locus, but could derive from the partial low expression of *Sp140*
265 and the loss of *Sp110* in B6.*Sst1*^{S}, as compared to the complete loss of functional SP140 protein
266 and retention of SP110 in *Sp140*$^{-/-}$ mice. Alternatively, the minor differences in gene expression
267 between B6.*Sst1*^{S} and B6.*Sp140*$^{-/-}$ mice could arise from additional genetic background or
268 microbiota differences between B6.*Sst1*^{S} and *Sp140*$^{-/-}$ mice. Interestingly, the gene most
269 significantly differentially expressed between B6.*Sst1*^{S} and *Sp140*$^{-/-}$ mice (i.e., with the smallest
270 adjusted *p*-value) was *Sp110* (Figure 4E). This result is expected, given that *Sp110* is not
271 expressed in B6.*Sst1*^{S} but is retained in our *Sp140*$^{-/-}$ mice (Figure 2 – figure supplement 1D).
272 Together, these results show that while they are not identical, the transcriptomes of *Sp140*$^{-/-}$ and
273 B6.*Sst1*^{S} mice greatly overlap during *M. tuberculosis* infection, and importantly, both strains
274 exhibit a similar type I IFN signature. Given the susceptibility of B6.*Sst1*^{S} mice is due to
275 overproduction of type I IFN (Ji et al., 2019), we hypothesized that type I IFNs might also
276 mediate the susceptibility of *Sp140*$^{-/-}$ mice.

277 **Susceptibility of *Sp140*$^{-/-}$ mice to bacterial infections is dependent on type I IFN signaling.**
278 To determine whether type I IFNs exacerbate *M. tuberculosis* infection of *Sp140*$^{-/-}$ mice, *M.*
279 *tuberculosis*-infected *Sp140*$^{-/-}$ mice were treated with a blocking antibody against IFNAR1.
280 Compared to mice that only received isotype control antibody, *Sp140*$^{-/-}$ mice that received the
281 anti-IFNAR1 antibody had reduced bacterial burdens in their lungs (Figure 5 – figure
282 supplement 1). We also generated *Sp140*$^{-/-}$*Ifnar*$^{-/-}$ double-deficient mice and infected them with
283 *M. tuberculosis* (Figure 5A-B). Loss of *Ifnar* protected *Sp140*$^{-/-}$ mice from weight loss (Figure
284 5A) and reduced bacterial burdens at day 25 post-infection, similar to those seen in B6 mice

285 (Figure 5B). Furthermore, *Sp140*$^{-/-}$*Ifnar*$^{-/-}$ mice were partially protected from *L. pneumophila*
286 infection, to a similar degree as B6.*Sst1*^{S}*Ifnar*$^{-/-}$ mice (Figure 5C-D). These results show that
287 similar to B6.*Sst1*^{S} mice, type I IFN signaling is responsible for the susceptibility of *Sp140*$^{-/-}$
288 mice to *M. tuberculosis*, and partially responsible for the susceptibility of *Sp140*$^{-/-}$ mice to *L.*
289 *pneumophila.*

290

291 **Discussion**

292 Humans and other vertebrates encounter diverse classes of pathogens, including viruses, bacteria,
293 fungi and parasites. In response, vertebrate immune systems have evolved stereotypical
294 responses appropriate for distinct pathogen types. For example, type I IFN-driven immunity is
295 generally critical for defense against viruses (Schneider et al., 2014; Stetson & Medzhitov,
296 2006), whereas type II IFN (IFN-γ)-driven immunity mediates resistance to intracellular
297 pathogens (Crisler & Lenz, 2018). Additionally, IL-1 is important for inducing neutrophil and
298 other responses against extracellular pathogens (Mantovani et al., 2019), and IL-4/-13 (Type 2
299 immunity) orchestrates responses to helminths and other parasites (Locksley, 1994). Thus, an
300 important question is how the immune system generates responses that are appropriate for
301 resistance to a specific pathogen while repressing inappropriate responses. The alternative
302 strategy of making all types of responses to all pathogens appears not to be employed, possibly
303 because it would be too energetically costly, or incur too much inflammatory damage to the host.
304 Although there is still much to be learned, it appears that negative feedback is essential to
305 enforce choices between possible types of immune responses. For example, IL-4 and IFN-γ have
306 long been appreciated to act as reciprocal negative antagonists of each other (Locksley, 1994). In
307 addition, anti-viral type I IFNs negatively regulate IFN-γ and IL-1-driven anti-bacterial
308 responses via diverse mechanisms (Donovan et al., 2017; Moreira-Teixeira et al., 2018).
309 Although negative regulation of IFN-γ/IL-1 by type I IFN is likely beneficial to limit
310 immunopathology during viral infections, *Sst1*^{S} mice provide an example of how excessive or
311 inappropriate negative regulation by type I IFN can also be detrimental during bacterial
312 infections (He et al., 2013; Ji et al., 2019). In this study, we therefore sought to understand the
313 molecular basis by which wild-type (*Sst1*^{R}) mice are able to restrain type I IFNs appropriately
314 during bacterial infections.

315 Although the *Sst1* locus was first described in 2005 (Pan et al., 2005), further genetic
316 analysis of the locus has been hindered by its extreme repetitiveness and the concomitant
317 difficulty in generating specific loss-of-function mutations in *Sst1*-linked genes. In particular, the
318 loss of *Sp110 (Ipr1)* has long been proposed to explain the susceptibility of *Sst1* mice to bacterial

319 infections. However, while we could confirm the loss of *Sp110* expression in *Sst1*^{S} mice, specific
320 *Sp110*$^{-/-}$ mice were never generated and thus its essential role in host defense has been unclear.
321 The advent of CRIPSR/Cas9-based methods of genome engineering allowed us to generate
322 *Sp110*$^{-/-}$ mice. Unexpectedly, we found *Sp110*$^{-/-}$ mice were fully resistant to *M. tuberculosis*
323 infection, and we thus conclude that lack of *Sp110* is not sufficient to explain the *Sst1*^{S}
324 phenotype. An important caveat of genetic studies of the *Sst1* locus is that generating specific
325 gene knockouts is still nearly impossible in this genetic region, even with CRISPR–Cas9. Indeed,
326 the guide sequence used to target exon 3 of *Sp110* also targets an unknown number of
327 pseudogene copies of *Sp110*-like genes located within the unassembled adjacent 'homogenously
328 staining region' of mouse chromosome 1. Thus, we expect that additional off-target mutations
329 are likely present in our *Sp110*$^{-/-}$ mutant mice. However, given that the *Sp110* pseudogenes are
330 not known to be expressed, we consider it unlikely that collateral mutations would affect our
331 conclusions. Moreover, any off-target mutations should differ among the three founder mice we
332 analyzed and are thus unlikely to explain the consistent resistant phenotype we observed in all
333 three founders. Additionally, we did not observe major changes in gene expression for other SP
334 family members (*Sp100, Sp140*) in *Sp110*$^{-/-}$ mice during *M. tuberculosis* infection (Figure 4 –
335 figure supplement 2). Lastly, since we were able to establish that all the founders at a minimum
336 lack SP110 protein, additional mutations would not affect our conclusion that *Sp110* is not
337 essential for resistance to *M. tuberculosis*.

338 Given that loss of *Sp110* was not sufficient to explain the susceptibility of *Sst1*^{S} mice to
339 bacterial infections, we considered other explanations. We found that *Sst1*^{S} mice also lack
340 expression of *Sp140*, an *Sst1*-linked homolog of *Sp110*. Our data suggest that deletion of *Sp140*
341 is sufficient to recapitulate the full *Sst1*^{S} phenotype including broad susceptibility to multiple
342 bacterial infections including *M. tuberculosis* and *L. pneumophila*. From analysis of RNA-seq
343 data generated from *M tuberculosis*-infected lungs, we found that the transcriptomes of *Sp140*$^{-/-}$
344 and B6.*Sst1*^{S} greatly overlap and display an elevated ISG signature. The elevated production of
345 *Ifnb* mRNA and *Il1rn* mRNA seen by RNAseq was validated by RT-qPCR. Enhanced *Ifnb*
346 production and *Ifnar*-dependent cell death was also observed during *in vitro* experiments with
347 BMMs. A causative role for type I IFNs in the phenotype of *Sp140*$^{-/-}$ and *Sst1*^{S} mice was seen in
348 the reduced susceptibility of *Sp140*$^{-/-}$*Ifnar*$^{-/-}$ and B6.*Sst1*^{S}*Ifnar*$^{-/-}$ mice to bacterial infection.
349 Overall, we therefore conclude that loss of *Sp140* likely explains the *Sst1*-linked hyper type I
350 IFN-driven susceptibility to bacterial infections. It remains possible that the additional loss of
351 *Sp110* in *Sst1*^{S} mice further exacerbates the *Sst1*^{S} susceptibility phenotype as compared to
352 *Sp140*$^{-/-}$ mice. However, in our studies, we did not observe a consistent difference in
353 susceptibility between *Sst1*^{S} (i.e., *Sp110*$^{-/-}$*Sp140*$^{-/-}$) mice as compared to our *Sp140*$^{-/-}$ mice.

354 Another important caveat to our study is that it remains possible that our *Sp140*$^{-/-}$ mice
355 carry additional mutations that contribute to, or even fully explain, their observed phenotype.
356 This concern is somewhat ameliorated by our analysis of two independent *Sp140*$^{-/-}$ founders,
357 both of which exhibited susceptibility to *M. tuberculosis* (Figure 2 – figure supplement 1E). We
358 confirmed there is normal SP110 protein levels in bone marrow macrophages from *Sp140*$^{-/-}$
359 mice (Figure 2 – figure supplement 1D), and normal levels of *Sp110* and *Sp100* mRNA in the
360 lungs of *M. tuberculosis*-infected *Sp140*$^{-/-}$ mice (Figure 4 – figure supplement 2). Thus,
361 collateral loss of SP100 or SP110 is unlikely to explain the phenotype of our *Sp140*$^{-/-}$ mice. To
362 address the possibility of mutations in unannotated SP-like genes, we used deep amplicon
363 sequencing of genomic DNA and cDNA from *Sp140*$^{-/-}$ mice. We confirmed that both founder
364 lines harbored distinct off-target mutations. Most of the identified off-target mutations are in
365 previously unidentified sequences that likely originate from *Sp140* paralogs within the unmapped
366 HSR. Most HSR-linked paralogs are believed to be pseudogenes, and indeed, the off-target
367 mutated genes appear to be expressed at a far lower level than *Sp140* in lungs during *M.*
368 *tuberculosis* infection. In one of our *Sp140*$^{-/-}$ lines, we identified an off-target mutated *Sp140*-
369 like paralog that was expressed at detectable levels in the lungs of *M. tuberculosis*-infected mice.
370 This paralog was 100% identical to *Sp140* in the sequenced region and was only distinguished
371 from *Sp140* itself because it lacked the deletion that was introduced into the edited *Sp140* gene.
372 Importantly, this previously undescribed *Sp140*-like expressed sequence was not mutated in our
373 second *Sp140*$^{-/-}$ line and is thus unlikely to explain resistance to *M. tuberculosis* infection. As an
374 alternative approach to confirm the phenotype of *Sp140*$^{-/-}$ mice is due to loss of *Sp140*, we
375 overexpressed *Sp140* in *Sp140*$^{-/-}$ BMMs. Crucially, we found *Sp140* complements aberrant
376 elevated *Ifnb* transcription exhibited by *Sp140*$^{-/-}$ BMMs upon TNFα stimulation. Lastly, *Sp110*
377 and *Sp140* are the only two *Sst1*-linked genes that we were able to find to be differentially
378 expressed between B6 and B6.*Sst1*^{S} mice, and as discussed above, our genetic studies suggest
379 little role for the loss of *Sp110*. Thus, while it is formally possible that an edited *Sp140* homolog
380 that was not identified by our amplicon sequencing contributes to the susceptibility to bacterial
381 infection and elevated type I IFN in *Sp140*$^{-/-}$ mice, the most parsimonious explanation of our
382 data is that deficiency in *Sp140* accounts for the *Sst1*^{S} phenotype. We expect that future
383 mechanistic studies will be critical to further confirm this conclusion.

384 Because *Sp140* is inducible by IFN-γ, our results suggest the existence of a novel
385 feedback loop by which IFN-γ acts to repress the transcription of type I IFNs via SP140. This
386 feedback loop appears to be essential for host defense against diverse bacterial pathogens. A
387 major question that remains is how SP140 acts to repress the type I IFN response. SP140
388 contains DNA/chromatin-binding domains, such as SAND, PHD and Bromodomains, which

389 suggests the hypothesis that SP140 functions as a direct transcriptional repressor of type I IFN
390 genes. However, much more indirect mechanisms are also possible. Recent studies suggest that
391 hyper type I IFN responses in TNF-stimulated B6.*Sst1*^{S} BMMs derive from aberrant oxidative
392 stress that activates the kinase JNK and ultimately results in a non-resolving stress response that
393 promotes necrosis (Bhattacharya et al., 2021; Brownhill et al., 2020). Interestingly, mouse SP140
394 localizes to nuclear structures called PML bodies. PML bodies are implicated in a variety of cell
395 processes such as apoptosis, cell cycle, DNA damage response, senescence, and cell-intrinsic
396 antiviral responses (Scherer & Stamminger, 2016). Whether or not the repressive effects of
397 SP140 on type I IFN expression occur via the activity of PML bodies is an important outstanding
398 question. Another major question is whether or how the repression of type I IFNs by SP140 is
399 specific for bacterial infections and, if not, whether the presence of SP140 impairs anti-viral
400 immunity. Lastly, polymorphisms in human SP140 are associated with chronic lymphocytic
401 leukemia (CLL), Crohn's disease and multiple sclerosis (MS) (Franke et al., 2010; Jostins et al.,
402 2012; Karaky et al., 2018; Matesanz et al., 2015; Slager et al., 2013). Studies using siRNA and
403 shRNA-mediated knockdown have also implicated SP140 in the repression of lineage-
404 inappropriate genes in macrophages (Mehta et al., 2017). Our generation of *Sp140*$^{-/-}$ mice is
405 therefore important to permit future studies into these alternative roles of SP140.

406

407 **Materials and Methods**

Key Resources Table				
Reagent type (species) or resource	**Designation**	**Source or reference**	**Identifiers**	**Additional information**
gene (*Mus musculus*)	*Sp110*	GenBank	Gene ID: 109032	
gene (*Mus musculus*)	*Sp140*	GenBank	Gene ID: 434484	
strain, strain background (*M. tuberculosis,* Erdman)	*M. tuberculosis*	Sarah Stanley, University of California, Berkeley	Erdman	

strain, strain background (*Legionella pneumophila*, JR32 ΔflaA)	*L. pneumophila*	Dario Zamboni, University of São Paulo, Brazil	JR32	
genetic reagent (*Mus musculus*)	*Sp110*$^{-/-}$	This paper		(C57BL/6J background)
genetic reagent (*Mus musculus*)	*Sp140*$^{-/-}$	This paper		(C57BL/6J background)
genetic reagent (*Mus musculus*)	B6.129S2-*Ifnar1*^{tm1Agt}/Mmjax	Jackson Laboratory	RRID:MMRRC_032045-JAX	
genetic reagent (*Mus musculus*)	B6J.C3-*Sst*$^{C3HeB/FeJ}$Krmn	Igor Kramnik, Boston University		
cell line (*Homo sapiens*)	GP-2 293	UC Berkeley Cell culture Facility	RRID:CVCL_WI48	
antibody	Rabbit anti-mouse SP110 (serum)	Covance, this paper		WB: 1:1000
antibody	Rabbit anti-mouse SP140 (serum)	Covance, this paper		WB: 1:1000
antibody	Mouse anti-mouse SP110 (hybridoma)	Igor Kramnik, Boston University		WB: 1:1000
antibody	Mouse anti-human IFNGR-α chain	Leinco Technologies, Inc	Cat #: GIR208	Mouse injection: 500 μg

	(isotype control)			
antibody	Mouse anti-mouse IFNAR1	Leinco Technologies, Inc	Cat #: MAR1-5A3	Mouse injection: 500 µg
recombinant DNA reagent	SINV-mincmvSp140-pgkAmetrine (plasmid)	This paper		Derived from pTMGP vector (Addgene plasmid # 32716, RRID:Addgene_32716)
recombinant DNA reagent	SINV-Gal4-mincmv-mNeonGreen-pgkAmetrine (plasmid)	This paper		Derived from pTMGP vector (Addgene plasmid # 32716, RRID:Addgene_32716)
recombinant DNA reagent	pMD2.G	Addgene	RRID:Addgene_12259 plasmid #32716	
peptide, recombinant protein	Recombinant murine TNFalpha	R&D Systems	Cat #: 410-TRNC-010	BMM stimulation: 10 ng/mL
peptide, recombinant protein	Recombinant murine interferon gamma	Biolegend	Cat #: 575304	BMM stimulation: 5 - 10 ng/mL
peptide, recombinant protein	Retronectin	Takara	T100	
sequence-based reagent	Sp110 fwd	This paper	Genotyping primers (*Sp110)*	CTCTCCGCTCGGTGACTAC

sequence-based reagent	Sp110 rev	This paper	Genotyping primers (*Sp110)*	CTGCACATGTGACAAGGATCTC
sequence-based reagent	Sp140-1 fwd	This paper	Genotyping primers (*Sp140)*	ACGAATAGCAAGCAGGAATGCT
sequence-based reagent	Sp140-1 rev	This paper	Genotyping primers (*Sp140)*	GGTTCCGGCTGAGCACTTAT
sequence-based reagent	Sp140-2 fwd	This paper	Genotyping primers (*Sp140)*	TGAGGACAGAACTCAGGGAG
sequence-based reagent	Sp140-2 rev	This paper	Genotyping primers (*Sp140)*	ACACGCCTTTAATCCCAGCATTT
sequence-based reagent	*Ifnb* sense	This paper	RT-qPCR primers (*Ifnb*)	GTCCTCAACTGCTCTCCACT
sequence-based reagent	*Ifnb* antisense	This paper	RT-qPCR primers (*Ifnb*)	CCTGCAACCACCACTCATTC
commercial assay or kit	E.Z.N.A. Total RNA Kit I	Omega Biotek	Cat #: R6834-02	
chemical compound, drug	polyI:C	Invivogen	Cat #: tlrl-picw	BMM stimulation: 100 μg/mL

408

409 **Mice.** All mice were specific pathogen-free, maintained under a 12-hr light-dark cycle (7AM to
410 7PM), and given a standard chow diet (Harlan irradiated laboratory animal diet) *ad libitum*. All
411 mice were sex and age-matched at 6-10 weeks old at the beginning of infections. C57BL/6J (B6)

412 and B6.129S2-*Ifnar1*^{tm1Agt}/Mmjax (*Ifnar*$^{-/-}$) were originally purchased from Jackson
413 Laboratories and subsequently bred at UC Berkeley. B6J.C3-*Sst* $^{C3HeB/FeJ}$Krmn mice (referred to
414 as B6.*Sst1*^{S} throughout) were from the colony of I. Kramnik at Boston University and then
415 transferred to UC Berkeley. CRISPR/Cas9 targeting was performed by pronuclear injection of
416 Cas9 mRNA and sgRNA into fertilized zygotes from colony-born C57BL/6J mice, essentially as
417 described previously (Wang et al., 2013). Founder mice were genotyped as described below, and
418 founders carrying *Sp140* mutations were bred one generation to C57BL/6J to separate modified
419 *Sp140* haplotypes. Homozygous lines were generated by interbreeding heterozygotes carrying
420 matched *Sp140* haplotypes. *Sp140*$^{-/-}$*Ifnar*$^{-/-}$ were generated by crossing the *Sp140*$^{-/-}$ and *Ifnar*$^{-/-}$
421 mice in-house. All animals used in experiments were bred in-house unless otherwise noted in the
422 figure legends. All animal experiments complied with the regulatory standards of, and were
423 approved by, the University of California Berkeley Institutional Animal Care and Use
424 Committee.

425 **Genotyping of *Sp110* alleles.** Exon 3 and the surrounding intronic regions were amplified by
426 PCR using the following primers (all 5' to 3'): Sp110 fwd, CTCTCCGCTCGGTGACTAC, and
427 rev, CTGCACATGTGACAAGGATCTC. The primer combinations were designed to
428 distinguish *Sp110* from other *Sp110*-like genes. Primers were used at 200 nM in each 20 µl
429 reaction with 1x Dreamtaq Green PCR Master Mix (Thermo Fisher Scientific). Cleaned PCR
430 products were diluted at 1:10 and sequenced using Sanger sequencing (Elim Biopharm).

431 **Genotyping of *Sp140* alleles.** Exon 3 and the surrounding intronic regions were amplified by
432 bracket PCR using the following primers (all 5′ to 3′): Sp140-1 fwd,
433 ACGAATAGCAAGCAGGAATGCT, and rev, GGTTCCGGCTGAGCACTTAT. The PCR
434 products are diluted at 1:10 and 2 µl were used as template for the second PCR using the
435 following primers: Sp140-2 fwd, TGAGGACAGAACTCAGGGAG, and rev,
436 ACACGCCTTTAATCCCAGCATTT. The primer combinations were designed to distinguish
437 *Sp140* from other *Sp140*-like genes. Primers were used at 200 nM in each 20 µl reaction with 1x
438 Dreamtaq Green PCR Master Mix (Thermo Fisher Scientific). Cleaned PCR products were
439 diluted at 1:10 and sequenced using Sanger sequencing (Elim Biopharm). PCRs were performed
440 as described above for *Sp110* and sequenced using Sanger sequencing (Elim Biopharm).

441 ***Mycobacterium tuberculosis* infections.** *M. tuberculosis* strain Erdman (gift of S.A. Stanley)
442 was used for all infections. Frozen stocks of this wild-type strain were made from a single
443 culture and used for all experiments. Cultures for infection were grown in Middlebrook 7H9
444 liquid medium supplemented with 10% albumin-dextrose-saline, 0.4% glycerol and 0.05%
445 Tween-80 for five days at 37°C. Mice were aerosol infected using an inhalation exposure system
446 (Glas-Col, Terre Haute, IN). A total of 9 ml of diluted culture was loaded into the nebulizer

447 calibrated to deliver ~20 to 50 bacteria per mouse as confirmed by measurement of colony
448 forming units (CFUs) in the lungs 1 day following infection. Mice were sacrificed at various
449 days post-infection (as described in figure legends) to measure CFUs and RNA levels. All but
450 one lung lobe was homogenized in PBS plus 0.05% Tween-80, and serial dilutions were plated
451 on 7H11 plates supplemented with 10% oleic acid, albumin, dextrose, catalase (OADC) and
452 0.5% glycerol. CFUs were counted 21 days after plating. The remaining lobe was used for
453 histology or for RNA extraction. For histology, the sample was fixed in 10% formalin for at least
454 48 hours then stored in 70% ethanol. Samples were sent to Histowiz Inc for embedding in wax,
455 sectioning and staining with hematoxylin and eosin. For histologic grading, slides were scanned
456 at 20X magnification and evaluated by a trained pathologist (S.N.) for the extent of macrophage,
457 lymphoid and granulocytic infiltration. The extent of infiltration was graded on a 0-4 scale with 0
458 being the least and 4 being the greatest. The extent of necrosis was similarly estimated. For
459 survival experiments, mice were monitored for weight loss and were euthanized when they
460 reached a humane endpoint as determined by the University of California Berkeley Institutional
461 Animal Care and Use Committee.

462 ***Legionella pneumophila* infections.** Infections were performed using *L. pneumophila* strain
463 JR32 Δ*flaA* (from the lab of D.S. Zamboni) as previously described (Goncalves et al., 2019;
464 Mascarenhas et al., 2015). Briefly, frozen cultures were streaked out on to BCYE plates to obtain
465 single colonies. A single colony was chosen and streaked on to a new BCYE plate to obtain a
466 1cm by 1cm square bacterial lawn, and incubated for 2 days at 37°C. The patch was solubilized
467 in autoclaved MilliQ water and the optical density was measured at 600 nm. Culture was diluted
468 to 2.5 x10^6 bacteria/ml in sterile PBS. The mice were first anesthetized with ketamine and
469 xylazine (90 mg/kg and 5 mg/kg, respectively) by intraperitoneal injection then infected
470 intranasally with 40 µL with PBS containing a final dilution of 1×10^5 bacteria per mouse. For
471 enumerating of CFU, the lungs were harvested and homogenized in 5 mL of autoclaved MilliQ
472 water for 30 seconds, using a tissue homogenizer. Lung homogenates were diluted in autoclaved
473 MilliQ water and plated on BCYE agar plates. CFU was enumerated after plates were incubated
474 for 4 days at 37°C.

475 **Bone marrow-derived macrophages (BMMs) and TNF-treatment**. Bone marrow was
476 harvested from mouse femurs and tibias, and cells were differentiated by culture on non-tissue
477 culture-treated plates in RPMI supplemented with supernatant from 3T3-MCSF cells (gift of B.
478 Beutler), 10% fetal bovine serum (FBS) (Gibco, CAT#16140071, LOT#1447825), 2mM
479 glutamine, 100 U/ml streptomycin and 100 µg/ml penicillin in a humidified incubator (37°C, 5%
480 CO_2). BMMs were harvested six days after plating and frozen in 95% FBS and 5% DMSO. For
481 *in vitro* experiments, BMMs were thawed into media as described above for 4 hours in a

482 humidified 37°C incubator. Adherent cells were washed with PBS, counted and replated at
483 $1.2x10^6$ - $1.5x10^6$ cells/well in a TC-treated 6-well plate. Cells were treated with 10 ng/ml
484 recombinant mouse TNFα (410-TRNC-010, R&D Systems) diluted in the media as described
485 above.

486 **Quantitative/conventional RT-PCR**. Total RNA from BMMs was extracted using E.Z.N.A.
487 Total RNA Kit I (Omega Bio-tek) according to manufacturer specifications. Total RNA from
488 infected tissues was extracted by homogenizing in TRIzol reagent (Life technologies) then
489 mixing thoroughly with chloroform, both done under BSL3 conditions. Samples were then
490 removed from the BSL3 facility and transferred to fresh tubes under BSL2 conditions. Aqueous
491 phase was separated by centrifugation and RNA was further purified using the E.Z.N.A. Total
492 RNA Kit I (Omega Bio-tek). Equal amounts of RNA from each sample were treated with DNase
493 (RQ1, Promega) and cDNA was made using Superscript III (Invitrogen). Complementary cDNA
494 reactions were primed with poly(dT) for the measurement of mature transcripts. For experiments
495 with multiple time points, macrophage samples were frozen in the RLT buffer (Qiagen) and
496 infected tissue samples in RNA*later*™ solution (Invitrogen) and processed to RNA at the same
497 time. Quantitative PCR was performed using QuantiStudio 5 Real-Time PCR System (Applied
498 Biosystems) with Power Sybr Green PCR Master Mix (Thermo Fisher Scientific) according to
499 manufacturer specifications. Transcript levels were normalized to housekeeping genes *Rps17,*
500 *Actb* and *Oaz1* unless otherwise specified. The following primers were used in this study. *Rps17*
501 sense: CGCCATTATCCC CAGCAAG; *Rps17* antisense: TGTCGGGATCCACCTCAATG;
502 *Oaz1* sense: GTG GTG GCC TCT ACA TCG AG; *Oaz1* antisense: AGC AGA TGA AAA CGT
503 GGT CAG; *Actb* sense: CGC AGC CAC TGT CGA GTC; *Actb* antisense: CCT TCT GAC CCA
504 TTC CCA CC; *Ifnb* sense: GTCCTCAACTGCTCTCCACT; *Ifnb* antisense:
505 CCTGCAACCACCACTCATTC; *Gbp4* sense: TGAGTACCTGGAGAATGCCCT; *Gbp4*
506 antisense: TGGCCGAATTGGATGCTTGG; *Ifit3* sense: AGCCCACACCCAGCTTTT; *Ifit3*
507 antisense: CAGAGATTCCCGGTTGACCT. *Tnfa* sense: TCTTCTCATTCCTGCTTGTGG;
508 *Tnfa* antisense: GGTCTGGGCCATAGAACTGA. Conventional RT-PCR shown in Figure 2A
509 used the following primers. Sense: GTCCCTTGGAGTCTGTGTAGG; antisense:
510 CATCCTGGGGCTCTTGTCTTG.

511 **Immunoblot.** Samples were lysed in RIPA buffer with protease inhibitor cocktail (Roche) to
512 obtain total protein lysate and were clarified by spinning at ~16,000×*g* for 30 min at 4°C.
513 Clarified lysates were analyzed with Pierce BCA protein assay kit (Thermo Fisher Scientific)
514 according to manufacturer specification and diluted to the same concentration and denatured
515 with SDS-loading buffer. Samples were separated on NuPAGE Bis–Tris 4% to 12% gradient
516 gels (Thermo Fisher Scientific) following the manufacturer's protocol. Gels were transferred

517 onto ImmobilonFL PVDF membranes at 35 V for 90 min and blocked with Odyssey blocking
518 buffer (Li-Cor). Proteins were detected on a Li-Cor Odyssey Blot Imager using the following
519 primary and secondary antibodies. Rabbit anti-SP110 or SP140 serums were produced by
520 Covance and used at 1:1000 dilution. Hybridoma cells expressing monoclonal anti-SP110
521 antibody were from the lab of I. Kramnik. Antibodies were produced in-house as previously
522 described (Ji et al., 2019) and used at 100 ng/ml. Alexa Fluor 680-conjugated secondary
523 antibodies (Invitrogen) were used at 0.4 mg/ml.

524 **RNA sequencing and analysis**. Total RNA was isolated as described above. Illumina-
525 compatible libraries were generated by the University of California, Berkeley, QB3 Vincent J.
526 Coates Genomics Sequencing Laboratory. PolyA selection was performed to deplete rRNA.
527 Libraries were constructed using Kapa Biosystem library preparation kits. The libraries were
528 multiplexed and sequenced using one flow cell on Novaseq 6000 (Illumina) as 50bp paired-end
529 reads. Base calling was performed using bcl2fastq2 v2.20. The sequences were aligned to mm10
530 genome using Kallisto v.0.46.0 using standard parameters (Pimentel et al., 2017) and analyzed
531 using Deseq2 (Love et al., 2014) and DEVis packages (Price et al., 2019). For Deseq2 and
532 DEVis analysis, all raw counts were incremented by 1 to avoid excluding genes due to division
533 by 0 in the normalization process, except for data shown in Figure 4 – figure supplement 2. Fold
534 changes were calculated with the apeglm shrinkage estimator (Zhu et al., 2019).

535 **Antibody-mediated neutralization**. Mice were given anti-IFNAR1 antibody or isotype control
536 once every 2 days, starting 7 days post-infection. All treatments were delivered by
537 intraperitoneal injection. Mouse anti-mouse IFNAR1 (MAR1-5A3) and isotype control (GIR208,
538 mouse anti-human IFNGR-α chain) were purchased from Leinco Technologies Inc. For
539 injections antibody stocks were diluted in sterile PBS and each mouse received 500 μg per
540 injection.

541 **Amplicon sequencing and analysis.** Amplicons comprising the 5'intron of exon 3 of *Sp140* and
542 the end of exon 3 were amplified from crude DNA from ear clips of B6 and *Sp140*$^{-/-}$1 mice
543 (sense: TCATATAACCCATAAATCCATCATGACA; antisense:
544 CCATTTAGGAAGAAGTGTTTTAGAGTCT) with PrimeStar PCR components (Takara,
545 R010b) for 18 cycles according to manufacturer specifications, then diluted 50-fold and
546 barcoded for an additional 18 cycles with Illumina-compatible sequencing adaptors. Amplicons
547 of *Sp140* exon 3 (sense: AATATCAAGAAACATGTAAGAACCTGGT; antisense:
548 CCATTTAGGAAGAAGTGTTTTAGAGTCT) and exon 2-3 (sense:
549 GCAGAAGTTTCAGGAATATCAAGAAACATGTAAG; antisense:
550 ACTTCTTCTGTACATTGCTGAGGATGT) were amplified from cDNA generated from lungs
551 of B6, both lines of *Sp140*$^{-/-}$ mice infected with *M. tuberculosis* for 25 cycles with PrimeStar

552 before barcoding. Libraries were generated by the University of California, Berkeley, QB3
553 Vincent J. Coates Genomics Sequencing Laboratory, and were multiplexed and sequenced on an
554 Illumina Miseq platform with v2 chemistry and 300 bp single-end reads for DNA amplicons, and
555 Illumina Miseq Nano platform with v3 chemistry for 300bp single end reads for cDNA
556 amplicons. Reads were aligned with Burrows-Wheeler Aligner (BWA-MEM) with default
557 parameters (Li, 2013; Li & Durbin, 2009) to chromosome 1 and non-localized genome contigs of
558 the *Mus musculus* genome (assembly mm10) as well as the *Sp140* gene and transcript
559 X1(XM_030255396.1), converted to BAM files with samtools (Li, 2009), and visualized in IGV
560 2.8. Subsets of reads were extracted from alignment files using the Seqkit toolkit (Shen et al.,
561 2016).

562 **Retroviral transduction of BMMs.** Self-inactivating pTMGP vector (SINV) with either a
563 minimal CMV promoter driving *Sp140* or a minimal CMV promoter and 4 Gal4 binding sites
564 driving mNeonGreen, and the reporter mAmetrine driven by a PGK promoter, were cloned using
565 Infusion (638910, Takara). pTGMP was from the lab of Scott Lowe (Addgene plasmid # 32716).
566 Virus was harvested from GP-2 cells transfected with SINV vectors and VSV-G (pMD2.G,
567 Addgene plasmid #12259) and grown in DMEM supplemented with 30% FBS and 2mM
568 glutamine, 100 U/ml streptomycin and 100 μg/ml penicillin (adapted from protocols described in
569 (Schmidt et al., 2015)). Harvested virus was concentrated 100-fold by ultracentrifugation in
570 RPMI before storage at -80 °C. Virus was thawed and titrated on bone marrow to optimize
571 transduction efficiency. Bone marrow was harvested as described above and the entirety of the
572 bone marrow was plated in a non-TC 15 cm plate. The next day, bone marrow was harvested and
573 transduced with SINV virus on plates coated with 10 μg/cm^2 Retronectin (T100, Takara) for 1.5-
574 2 hrs at 650×*g* and 37°C. After 2 days of additional culture, media was replenished, then
575 transduced bone marrow was cultured for 3 additional days before sorting. Sorted transduced
576 macrophages were stimulated with 5 ng/mL recombinant murine IFN-γ (575304, Biolegend) 12-
577 14 hours before stimulation with 10 ng/mL recombinant TNFα as described above for 4 hours
578 (FBS used in these experiments was from Omega, LOT 721017, CAT# FB-12). RNA isolation
579 and RT-qPCR were performed as described above. No mycoplasma contamination was detected
580 by PCR in GP-2 cells used for these experiments (sense: CACCATCTGTCACTCTGTTAACC;
581 antisense: GGAGCAAACAGGATTAGATACCC), and GP-2 cells were authenticated by short
582 tandem repeat DNA profiling by the UC Berkeley DNA Sequencing Facility.

583 **Quantification of cell death upon polyI:C treatment.** Day 6-7 primary BMMs were derived
584 from fresh or frozen bone marrow as described above. BMMs were plated at 50,000-90,000 cells
585 per well in 96 well non-TC treated plates, and stimulated for 16-24 hours with 100 μg/mL
586 polyI:C (tlrl-picw, Invivogen). LDH assays were performed on supernatants after stimulation as

587 previously described (Decker, 1988). Similar results were obtained for BMMs cultured with FBS
588 from Omega and Gibco (LOT 721017, CAT# FB-12, and LOT# 1447825, CAT#16140071
589 respectively).

590 **Statistical analysis**. All data were analyzed with Mann-Whitney test unless otherwise noted.
591 Tests were run using GraphPad Prism 5. *, $p \leq 0.05$; **, $p \leq 0.01$; ***, $p \leq 0.005$. All error bars
592 are s.e. Figures show exact p values for $p > 0.0005$.

593 **Data accession.** RNA-seq data is available at GEO, accession number GSE166114. Amplicon
594 sequencing data is available at the SRA, BioProject accession number PRJNA698382.

595 **Acknowledgements:** We thank the Stanley and Cox laboratories for support with *M.*
596 *tuberculosis* experiments, L. Flores, P. Dietzen and R. Chavez for technical assistance, and
597 members of the Vance, Barton, Cox, Stanley, and Portnoy labs for advice and discussions.

598 **Author contributions:** Conceptualization–D.X.J., K.H.D., A.Y.L., R.E.V., K.C.W., I.K.,
599 D.A.P.; Formal analysis–D.X.J., K.C.W; Investigation– D.X.J., KC.W., D.I.K., S.R.M., A.L.,
600 V.C., K.C., M.G., H.D., A.Y.L., S.N., D.S.Z.; Validation– K.C.W., D.I.K., S.N.,V.C.;
601 Methodology–D.X.J., K.C.W., D.I.K., S.R.M., A.L., V.C., M.G., H.D., S.N., K.J.C., A.Y.L.,
602 D.S.Z., K.H.D.; Resources–I.K., D.A.P., R.E.V.; Data curation–D.X.J., K.C.W.; Writing –
603 original draft preparation–D.X.J., R.E.V., K.C.W; Writing – review & editing–D.X.J., K.C.W.,
604 D.I.K., S.R.M., K.H.D., R.E.V., D.S.Z., I.K.; Supervision–D.A.P., K.H.D., A.Y.L., D.S.Z.,
605 R.E.V.; Funding acquisition–D.A.P., K.H.D., R.E.V. Project administration–D.A.P., R.E.V.

606 **Funding**: R.E.V. is supported by an Investigator Award from the Howard Hughes Medical
607 Institute. This work was also supported by NIH grants R37AI075039 and R01AI155634
608 (R.E.V.), P01AI066302 (R.E.V. and D.A.P.). R.E.V. and K.H.D. were Burroughs Wellcome
609 Fund Investigators in the Pathogenesis of Infectious Disease.

610 **Competing Interests**: R.E.V. consults for Ventus Therapeutics.

611 **Ethics Statement**: Animal studies were approved by the UC Berkeley Animal Care and Use
612 Committee.

613

614

615 **Figure Legends**

616 **Figure 1. *Sp110*$^{-/-}$ mice are not susceptible to *M. tuberculosis* infections.** (**A**) BMMs were
617 treated with 10 U/ml of IFNγ for 24 hours and cells were lysed with RIPA buffer. Five μg of
618 total protein was loaded on each lane, and immunoblot was performed with respective antibodies
619 as shown. Molecular weight standards are shown on the left of each blot in kDa. Individual
620 membranes were imaged separately. Three independent lines of *Sp110*$^{-/-}$ mice were analyzed
621 (denoted lines 61, 65, and 71). (**B-D**), Lungs of mice infected with *M. tuberculosis* were stained
622 with hematoxylin and eosin (H&E) for histology (**B**), measured for CFU at 25 days post-
623 infection (Mann-Whitney test) (**C**) or, monitored for survival (**D**). All except B6 mice were bred
624 in-house, and combined results from the three independent *Sp110*$^{-/-}$ lines are shown.
625 Representative of 2 experiments (**B, D**); combined results of 3 infections (**C**). *, $p \leq 0.05$; **, p
626 ≤ 0.01; ***, $p \leq 0.005$.

627 **Figure 2. *Sp140*$^{-/-}$ mice are susceptible to bacterial pathogens.** (**A**) RT-PCR of cDNA from
628 BMMs of the indicated genotypes. Red arrow indicates band corresponding to a portion of
629 *Sp140*, verified by sequencing. (**B**) Immunoblot of lysates from *Sp140*$^{-/-}$ and WT BMMs treated
630 with 10 U/ml of recombinant mouse IFNγ for 24 hours. Equal amounts of protein were loaded
631 for immunoblot with anti-SP140 antibody. (**C-F**) Mice were infected with *M. tuberculosis* and
632 measured for (**C**) lung CFU at 28 days post-infection, (**E**) body weight over time, and (**F**)
633 survival. Statistics in (**E**) shows comparison to B6 at day 28, and data are from 10 B6, 11
634 B6.*Sst1*^{S}, 11 *Sp110*$^{-/-}$, 14 *Sp140*$^{-/-}$, and 6 *Sp140*$^{+/-}$mice. (**D**) H&E staining of lungs at 25 days
635 post-infection with *M. tuberculosis*. Full histology images are provided in Figure 2 – figure
636 supplement 2. (**G**) Mice were infected with *L. pneumophila* and lung CFUs were determined at
637 96 hours post-infection. All mice were bred in-house, *Sp140*$^{-/-}$ and *Sp140*$^{+/-}$ were littermates (**C-**
638 **F**). **C**, **E**, and **G** are combined results of two independent infections. **A-D** shows representative
639 analysis of one *Sp140*$^{-/-}$ line (line 1), whereas **F-G** includes a mixture of both lines 1 and 2.
640 Results of infection of both lines with *M. tuberculosis* is shown in Figure 2 – figure supplement
641 1E. (**C, E, F, G**) Mann-Whitney test. *, $p \leq 0.05$; **, $p \leq 0.01$; ***, $p \leq 0.005$.

642 **Figure 3. *Sp140*$^{-/-}$ mice have elevated *Ifnb* transcripts during bacterial infection.** (**A**) Mice
643 were infected with *M. tuberculosis* and at 28 days post-infection lungs were processed for total
644 RNA, which was used for RT-qPCR. Combined results of 2 independent experiments. (**B**) Mice
645 were infected with *L. pneumophila* and RT-qPCR (top panel) and CFU enumeration (bottom
646 panel) was performed on lungs collected at indicated times. Combined results of 2 independent
647 infections. All mice were bred in-house, *Sp140*$^{-/-}$ and *Sp140*$^{+/-}$ were littermates. (**A-B**) Mann-
648 Whitney test. *, $p \leq 0.05$; **, $p \leq 0.01$; ***, $p \leq 0.005$.

649 **Figure 4. Global gene expression analysis of *Sp110*$^{-/-}$, *Sp140*$^{-/-}$ and B6.*Sst1*^{S} lungs after *M.***
650 ***tuberculosis* infection.** (**A**) PCA or (**B**) Euclidean distance analysis of all the samples. (**C-D**)
651 heatmaps of gene expression in $\log_2$-fold change from *M.* tuberculosis-infected B6. Genes shown
652 are those significantly different between *Sp140*$^{-/-}$ and B6: (**C**) GSEA Hallmark inflammatory
653 response; and (**D**) GO type I IFN response genes. (**E**) Volcano plot comparing *Sp140*$^{-/-}$ to
654 B6.*Sst1*^{S} expression. Dots in red are 2-fold differentially expressed with adjusted p-value ≤ 0.05.

655 **Figure 5. Susceptibility of *Sp140*$^{-/-}$ to *M. tuberculosis* and *L. pneumophila* is dependent on**
656 **type I IFN signaling**. (**A-B**) mice were infected with *M. tuberculosis* and measured for (**A**) body
657 weight, and (**B**) bacterial burdens at day 25. Statistics in **A** show comparison to B6; data are from
658 9 B6, 13 *Sp140*$^{-/-}$, and *Sp140*$^{-/-}$ *Ifnar*$^{-/-}$ mice. Combined results of 2 experiments. (**C-D**)
659 bacteria burden in *L. pneumophila*-infected mice at 96 hours. Combined results of 2 experiments.
660 All mice were bred in-house (**A-B**, **D**); all but B6 were bred in-house (**C**). Mann-Whitney test
661 (**A-D**). *, $p \leq 0.05$; **, $p \leq 0.01$; ***, $p \leq 0.005$.

662 **Figure 1 – figure supplement 1. CRISPR–Cas9 targeting strategy for *Sp110*$^{-/-}$ mice.** (**A**)
663 Mouse *Sp110* gene. Guide RNA sequence for CRISPR–Cas9 targeting and protospacer-adjacent
664 motif (PAM) are indicated. (**B-D**) *Sp110* locus in wildtype (WT) and three independent lines.
665 Homozygotes of 2 lines identified by sequencing (**B-C**), and heterozygote of the 3rd line by PCR
666 products separated on an agarose gel (**D**). Arrow indicates the mutant band.

667 **Figure 2 – figure supplement 1. CRISPR–Cas9 targeting strategy for *Sp140*$^{-/-}$ and**
668 **validation of founders.** (**A**) Mouse *Sp140* gene. Guide RNA sequence for CRISPR–Cas9
669 targeting and protospacer-adjacent motif (PAM) are indicated. (**B-C**) *Sp140* locus in wildtype
670 (WT) and 2 independent founders of *Sp140*$^{-/-}$ validated by sequencing. (**D**) Immunoblot for
671 SP110 using BMMs from mice of the indicated genotypes. Intervening lanes have been removed
672 for clarity (indicated by line in the image). (**E**) *M. tuberculosis*-infected mice were harvested for
673 CFU at 25 days post-infection. Empty and filled triangles indicate the two independent lines of
674 *Sp140*$^{-/-}$ used in this infection. All mice were bred in-house and *Sp140*$^{+/-}$ were littermates with
675 *Sp140*$^{-/-}$ line 2. Mann-Whitney test, *, $p \leq 0.05$; **, $p \leq 0.01$; ***, $p \leq 0.005$.

676 **Figure 2 – figure supplement 2. Histology of lungs from B6, B6.*Sst1*^{S}, *Sp110*$^{-/-}$, *Sp140*$^{-/-}$**
677 **mice after infection with *M. tuberculosis.*** H&E staining of entire lung sections from mice of
678 indicated genotypes at 25 days post-infection with *M. tuberculosis.* Black squares denote
679 sections shown in Figure 2C. Each image represents a lung section from a different mouse.
680 Borders in background color have been added around each image. Scale bar applies to all
681 images. Samples were evaluated and scored (0-4, least to most) for macrophage (histocyte),
682 lymphoid, granulocyte infiltration, and extent of necrosis.

683 **Figure 2 – figure supplement 3. Characterization of off-target genes mutated in *Sp140*$^{-/-}$**
684 **mice.** (**A**) Schematic of amplicon sequencing strategy for *Sp140* and *Sp140* homologs. (B)
685 Summary of edited *Sp140* homologs from amplicon sequencing and RNA-seq analysis. SNPs are
686 denoted based on the *Sp140* X1 transcript. Expression level was roughly estimated from read
687 counts. Three B6 and 2 *Sp140*$^{-/-}$ mice from each founder line were used as biological replicates
688 for *Sp140* exon 2/3 amplicon sequencing from cDNA, 2 mice per genotype were used for *Sp140*
689 exon 3 amplicon sequencing from cDNA, and 1 mouse per genotype was used for *Sp140* exon 3
690 amplicon sequencing from DNA.

691 **Figure 2 – figure supplement 4. Complementation of hyper type I IFN responses in *Sp140*$^{-}$**
692 **$^{/-}$ BMMs.** (**A**) BMMs were left untreated or treated with TNF-α for 24 hours. Total RNA was
693 used for RT-qPCR. Averages of technical duplicates for one biological replicate are shown. Data
694 is representative of two independent experiments. (**B**) RT-qPCR of *Sp140*$^{-/-}$ BMMs transduced
695 with either control SINV-minCMV-GAL4-mNeonGreen (SINV-mNeonGreen) or SINV-
696 minCMV-Sp140 (SINV-Sp140), primed with 5 ng/mL IFN-γ for 14 hours and treated with 10
697 ng/mL TNF-α for 4 hours. *, $p \leq 0.05$ calculated with an unpaired t-test with Welch's
698 correction. Data are representative of two independent experiments.

699 **Figure 3 – figure supplement 1. BMMs from B6.*Sst1*^{S} and *Sp140*$^{-/-}$ mice show increased cell**
700 **death upon stimulation with polyI:C, which is dependent upon IFNAR signaling.** LDH
701 release from primary BMMs after 16-24 hour stimulation with 100 µg/mL polyI:C for (**A**) B6,
702 *Sp140*$^{-/-}$, B6.*Sst1*^{S}, and B6.*Sst1*^{S}*Ifnar*$^{-/-}$ mice. Results are technical duplicates, and representative
703 of three independent experiments for B6 (3 mice), B6.*Sst1*^{S} (2 mice), and *Sp140*$^{-/-}$ (2 mice)
704 samples and two independent experiments for B6.*Sst1*^{S}*Ifnar*$^{-/-}$ sample (1 mouse). (**B**) LDH
705 release after polyI:C stimulation for primary BMMs from B6, *Sp140*$^{-/-}$, and *Sp140*$^{-/-}$*Ifnar*$^{-/-}$
706 mice. Results represent technical triplicates and are representative of two independent
707 experiments for two mice per genotype. *, $p \leq 0.05$; **, $p \leq 0.01$; ***, $p \leq 0.005$ as calculated
708 with an unpaired t-test with Welch's correction.

709 **Figure 4 – figure supplement 1. B6.*Sst1*^{S} and *Sp140*$^{-/-}$ lungs exhibit elevated transcript**
710 **levels of the interferon stimulated gene *Il1rn* during *M. tuberculosis infection.*** RT-qPCR for
711 *Il1rn* (encodes IL-1Ra) extracted from lungs at 28 days post-infection with *M. tuberculosis.*
712 Combined results of two independent experiments. Mann-Whitney test, *, $p \leq 0.05$; **, $p \leq$
713 0.01; ***, $p \leq 0.005$.

714 **Figure 4 – figure supplement 2. Expression of SP family members in *Sp140*$^{-/-}$ and *Sp110*$^{-/-}$**
715 **mouse lungs during *M. tuberculosis* infection.** Log_2-fold change and adjusted *p*-value for SP

716 family members (*Sp100, Sp110, Sp140)* from RNA-seq of *M. tuberculosis*-infected lungs from
717 *Sp110*$^{-/-}$ and *Sp140*$^{-/-}$ mice, compared to B6 and B6.*Sst1*^{S}.

718 **Figure 5 – figure supplement 1. Antibody blockade of IFNAR1 reduces bacterial burden in**
719 ***Sp140*$^{-/-}$ mice during *M. tuberculosis* infection.** Mice were infected with *M. tuberculosis* and
720 treated with either IFNAR1-blocking antibody or isotype control starting 7 days post-infection.
721 At 25 days post-infection lungs were harvested to enumerate CFU. Results of one experiment.
722 All mice were bred in-house. Mann-Whitney test, *, $p \leq 0.05$; **, $p \leq 0.01$; ***, $p \leq 0.005$.

723

724

725

726 **References**

727 Anderson, M. S., & Su, M. A. (2016). AIRE expands: new roles in immune tolerance and
728 beyond. *Nat Rev Immunol*, *16*(4), 247-258. https://doi.org/10.1038/nri.2016.9
729 Auerbuch, V., Brockstedt, D. G., Meyer-Morse, N., O'Riordan, M., & Portnoy, D. A. (2004).
730 Mice lacking the type I interferon receptor are resistant to Listeria monocytogenes. *J Exp Med*,
731 *200*(4), 527-533. https://doi.org/10.1084/jem.20040976
732 Bhattacharya, B., Xiao, S., Chatterjee, S., Urbanowski, M., Ordonez, A., Ihms, E. A., Agrahari,
733 G., Lun, S., Berland, R., Pichugin, A., Gao, Y., Connor, J., Ivanov, A. R., Yan, B. S., Kobzik,
734 L., Koo, B. B., Jain, S., Bishai, W., & Kramnik, I. (2021). The integrated stress response
735 mediates necrosis in murine Mycobacterium tuberculosis granulomas. *Journal of Clinical*
736 *Investigation*, *131*(3). https://doi.org/10.1172/JCI130319
737 Bottomley, M. J., Collard, M. W., Huggenvik, J. I., Liu, Z., Gibson, T. J., & Sattler, M. (2001).
738 The SAND domain structure defines a novel DNA-binding fold in transcriptional regulation.
739 *Nat Struct Biol*, *8*(7), 626-633. https://doi.org/10.1038/89675
740 Boxx, G. M., & Cheng, G. (2016). The Roles of Type I Interferon in Bacterial Infection. *Cell*
741 *Host Microbe*, *19*(6), 760-769. https://doi.org/10.1016/j.chom.2016.05.016
742 Boyartchuk, V., Rojas, M., Yan, B. S., Jobe, O., Hurt, N., Dorfman, D. M., Higgins, D. E.,
743 Dietrich, W. F., & Kramnik, I. (2004). The host resistance locus sst1 controls innate immunity
744 to Listeria monocytogenes infection in immunodeficient mice. *J Immunol*, *173*(8), 5112-5120.
745 https://doi.org/10.4049/jimmunol.173.8.5112
746 Brownhill, E., Yabaji, S. M., Zhernovkov, V., Rukhlenko, O. S., Seidel, K., Bhattacharya, B.,
747 Chatterjee, S., Chen, H. A., Crossland, N., Bishai, W., Kholodenko, B. N., Gimelbrant, A.,
748 Kobzik, L., & Kramnik, I. (2020). Maladaptive oxidative stress cascade drives type I interferon
749 hyperactivity in TNF activated macrophages promoting necrosis in murine tuberculosis
750 granulomas. *bioRxiv*, 2020.2012.2014.422743. https://doi.org/10.1101/2020.12.14.422743
751 Carrero, J. A., Calderon, B., & Unanue, E. R. (2004). Type I interferon sensitizes lymphocytes to
752 apoptosis and reduces resistance to Listeria infection. *J Exp Med*, *200*(4), 535-540.
753 https://doi.org/10.1084/jem.20040769
754 Chang, S. Y., Chen, M. L., Lee, M. R., Liang, Y. C., Lu, T. P., Wang, J. Y., & Yan, B. S. (2018).
755 SP110 Polymorphisms Are Genetic Markers for Vulnerability to Latent and Active
756 Tuberculosis Infection in Taiwan. *Dis Markers*, *2018*, 4687380.
757 https://doi.org/10.1155/2018/4687380
758 Crisler, W. J., & Lenz, L. L. (2018). Crosstalk between type I and II interferons in regulation of
759 myeloid cell responses during bacterial infection. *Curr Opin Immunol*, *54*, 35-41.
760 https://doi.org/10.1016/j.coi.2018.05.014
761 Decker, T., & Lohmann-Matthes, M. L. (1988). A quick and simple method for the quantitation
762 of lactate dehydrogenase release in measurements of cellular cytotoxicity and tumor necrosis
763 factor (TNF) activity. *Journal of immunological methods*, *115*(1), 61-69.
764 Donovan, M. L., Schultz, T. E., Duke, T. J., & Blumenthal, A. (2017). Type I Interferons in the
765 Pathogenesis of Tuberculosis: Molecular Drivers and Immunological Consequences. *Front*
766 *Immunol*, *8*, 1633. https://doi.org/10.3389/fimmu.2017.01633
767 Dorhoi, A., Yeremeev, V., Nouailles, G., Weiner, J., 3rd, Jorg, S., Heinemann, E., Oberbeck-
768 Muller, D., Knaul, J. K., Vogelzang, A., Reece, S. T., Hahnke, K., Mollenkopf, H. J.,
769 Brinkmann, V., & Kaufmann, S. H. (2014). Type I IFN signaling triggers immunopathology in
770 tuberculosis-susceptible mice by modulating lung phagocyte dynamics. *Eur J Immunol*, *44*(8),
771 2380-2393. https://doi.org/10.1002/eji.201344219

772 Fox, G. J., Sy, D. N., Nhung, N. V., Yu, B., Ellis, M. K., Van Hung, N., Cuong, N. K., Thi Lien,
773 L., Marks, G. B., Saunders, B. M., & Britton, W. J. (2014). Polymorphisms of SP110 are
774 associated with both pulmonary and extra-pulmonary tuberculosis among the Vietnamese.
775 *PLoS One*, *9*(7), e99496. https://doi.org/10.1371/journal.pone.0099496
776 Franke, A., McGovern, D. P., Barrett, J. C., Wang, K., Radford-Smith, G. L., Ahmad, T., Lees,
777 C. W., Balschun, T., Lee, J., Roberts, R., Anderson, C. A., Bis, J. C., Bumpstead, S.,
778 Ellinghaus, D., Festen, E. M., Georges, M., Green, T., Haritunians, T., Jostins, L., Latiano, A.,
779 Mathew, C. G., Montgomery, G. W., Prescott, N. J., Raychaudhuri, S., Rotter, J. I., Schumm,
780 P., Sharma, Y., Simms, L. A., Taylor, K. D., Whiteman, D., Wijmenga, C., Baldassano, R. N.,
781 Barclay, M., Bayless, T. M., Brand, S., Buning, C., Cohen, A., Colombel, J. F., Cottone, M.,
782 Stronati, L., Denson, T., De Vos, M., D'Inca, R., Dubinsky, M., Edwards, C., Florin, T.,
783 Franchimont, D., Gearry, R., Glas, J., Van Gossum, A., Guthery, S. L., Halfvarson, J.,
784 Verspaget, H. W., Hugot, J. P., Karban, A., Laukens, D., Lawrance, I., Lemann, M., Levine,
785 A., Libioulle, C., Louis, E., Mowat, C., Newman, W., Panes, J., Phillips, A., Proctor, D. D.,
786 Regueiro, M., Russell, R., Rutgeerts, P., Sanderson, J., Sans, M., Seibold, F., Steinhart, A. H.,
787 Stokkers, P. C., Torkvist, L., Kullak-Ublick, G., Wilson, D., Walters, T., Targan, S. R., Brant,
788 S. R., Rioux, J. D., D'Amato, M., Weersma, R. K., Kugathasan, S., Griffiths, A. M., Mansfield,
789 J. C., Vermeire, S., Duerr, R. H., Silverberg, M. S., Satsangi, J., Schreiber, S., Cho, J. H.,
790 Annese, V., Hakonarson, H., Daly, M. J., & Parkes, M. (2010). Genome-wide meta-analysis
791 increases to 71 the number of confirmed Crohn's disease susceptibility loci. *Nat Genet*, *42*(12),
792 1118-1125. https://doi.org/10.1038/ng.717
793 Fraschilla, I., & Jeffrey, K. L. (2020). Special Issue: Molecular Mechanisms of Immunity The
794 Speckled Protein (SP) Family: Immunity's Chromatin Readers. *Trends in Immunology*, *41*,
795 572-585. https://doi.org/10.1016/j.it.2020.04.007
796 Goncalves, A. V., Margolis, S. R., Quirino, G. F. S., Mascarenhas, D. P. A., Rauch, I., Nichols,
797 R. D., Ansaldo, E., Fontana, M. F., Vance, R. E., & Zamboni, D. S. (2019). Gasdermin-D and
798 Caspase-7 are the key Caspase-1/8 substrates downstream of the NAIP5/NLRC4
799 inflammasome required for restriction of Legionella pneumophila. *PLoS Pathog*, *15*(6),
800 e1007886. https://doi.org/10.1371/journal.ppat.1007886
801 Harper, J., Skerry, C., Davis, S. L., Tasneen, R., Weir, M., Kramnik, I., Bishai, W. R., Pomper,
802 M. G., Nuermberger, E. L., & Jain, S. K. (2012). Mouse model of necrotic tuberculosis
803 granulomas develops hypoxic lesions. *J Infect Dis*, *205*(4), 595-602.
804 https://doi.org/10.1093/infdis/jir786
805 He, X., Berland, R., Mekasha, S., Christensen, T. G., Alroy, J., Kramnik, I., & Ingalls, R. R.
806 (2013). The sst1 resistance locus regulates evasion of type I interferon signaling by Chlamydia
807 pneumoniae as a disease tolerance mechanism. *PLoS Pathog*, *9*(8), e1003569.
808 https://doi.org/10.1371/journal.ppat.1003569
809 Huoh, Y. S., Wu, B., Park, S., Yang, D., Bansal, K., Greenwald, E., Wong, W. P., Mathis, D., &
810 Hur, S. (2020). Dual functions of Aire CARD multimerization in the transcriptional regulation
811 of T cell tolerance. *Nature Communications*, *11*(1). https://doi.org/10.1038/s41467-020-15448-
812 w
813 Ji, D. X., Yamashiro, L. H., Chen, K. J., Mukaida, N., Kramnik, I., Darwin, K. H., & Vance, R.
814 E. (2019). Type I interferon-driven susceptibility to Mycobacterium tuberculosis is mediated
815 by IL-1Ra. *Nat Microbiol*, *4*(12), 2128-2135. https://doi.org/10.1038/s41564-019-0578-3
816 Jostins, L., Ripke, S., Weersma, R. K., Duerr, R. H., McGovern, D. P., Hui, K. Y., Lee, J. C.,
817 Schumm, L. P., Sharma, Y., Anderson, C. A., Essers, J., Mitrovic, M., Ning, K., Cleynen, I.,

818 Theatre, E., Spain, S. L., Raychaudhuri, S., Goyette, P., Wei, Z., Abraham, C., Achkar, J. P.,
819 Ahmad, T., Amininejad, L., Ananthakrishnan, A. N., Andersen, V., Andrews, J. M., Baidoo,
820 L., Balschun, T., Bampton, P. A., Bitton, A., Boucher, G., Brand, S., Buning, C., Cohain, A.,
821 Cichon, S., D'Amato, M., De Jong, D., Devaney, K. L., Dubinsky, M., Edwards, C.,
822 Ellinghaus, D., Ferguson, L. R., Franchimont, D., Fransen, K., Gearry, R., Georges, M.,
823 Gieger, C., Glas, J., Haritunians, T., Hart, A., Hawkey, C., Hedl, M., Hu, X., Karlsen, T. H.,
824 Kupcinskas, L., Kugathasan, S., Latiano, A., Laukens, D., Lawrance, I. C., Lees, C. W., Louis,
825 E., Mahy, G., Mansfield, J., Morgan, A. R., Mowat, C., Newman, W., Palmieri, O., Ponsioen,
826 C. Y., Potocnik, U., Prescott, N. J., Regueiro, M., Rotter, J. I., Russell, R. K., Sanderson, J. D.,
827 Sans, M., Satsangi, J., Schreiber, S., Simms, L. A., Sventoraityte, J., Targan, S. R., Taylor, K.
828 D., Tremelling, M., Verspaget, H. W., De Vos, M., Wijmenga, C., Wilson, D. C., Winkelmann,
829 J., Xavier, R. J., Zeissig, S., Zhang, B., Zhang, C. K., Zhao, H., International, I. B. D. G. C.,
830 Silverberg, M. S., Annese, V., Hakonarson, H., Brant, S. R., Radford-Smith, G., Mathew, C.
831 G., Rioux, J. D., Schadt, E. E., Daly, M. J., Franke, A., Parkes, M., Vermeire, S., Barrett, J. C.,
832 & Cho, J. H. (2012). Host-microbe interactions have shaped the genetic architecture of
833 inflammatory bowel disease. *Nature*, *491*(7422), 119-124. https://doi.org/10.1038/nature11582
834 Karaky, M., Fedetz, M., Potenciano, V., Andres-Leon, E., Codina, A. E., Barrionuevo, C.,
835 Alcina, A., & Matesanz, F. (2018). SP140 regulates the expression of immune-related genes
836 associated with multiple sclerosis and other autoimmune diseases by NF-kappaB inhibition.
837 *Hum Mol Genet*, *27*(23), 4012-4023. https://doi.org/10.1093/hmg/ddy284
838 Lei, X., Zhu, H., Zha, L., & Wang, Y. (2012). SP110 gene polymorphisms and tuberculosis
839 susceptibility: a systematic review and meta-analysis based on 10 624 subjects. *Infect Genet*
840 *Evol*, *12*(7), 1473-1480. https://doi.org/10.1016/j.meegid.2012.05.011
841 Li, H. (2013). *Aligning sequence reads, clone sequences and assembly contigs with BWA-MEM*.
842 http://arxiv.org/abs/1303.3997
843 Li, H., & Durbin, R. (2009). Fast and accurate short read alignment with Burrows-Wheeler
844 transform. *Bioinformatics*, *25*(14), 1754-1760. https://doi.org/10.1093/bioinformatics/btp324
845 Li, H., Handsaker, B., Wysoker, A., Fennell, T., Ruan, J., Homer, N., Marth, G., Abecasis, G.,
846 Durbin, R., & 1000 Genome Project Data Processing Subgroup. (2009). The Sequence
847 Alignment/Map format and SAMtools. *Bioinformatics (Oxford, England)*, *25*(16), 2078–2079.
848 https://doi.org/https://doi.org/10.1093/bioinformatics/btp352
849 Locksley, R. M. (1994). Th2 cells: help for helminths. *J Exp Med*, *179*(5), 1405-1407.
850 https://doi.org/10.1084/jem.179.5.1405
851 Love, M. I., Huber, W., & Anders, S. (2014). Moderated estimation of fold change and
852 dispersion for RNA-seq data with DESeq2. *Genome Biol*, *15*(12), 550.
853 https://doi.org/10.1186/s13059-014-0550-8
854 Mantovani, A., Dinarello, C. A., Molgora, M., & Garlanda, C. (2019). Interleukin-1 and Related
855 Cytokines in the Regulation of Inflammation and Immunity. *Immunity*, *50*(4), 778-795.
856 https://doi.org/10.1016/j.immuni.2019.03.012
857 Mascarenhas, D. P., Pereira, M. S., Manin, G. Z., Hori, J. I., & Zamboni, D. S. (2015).
858 Interleukin 1 receptor-driven neutrophil recruitment accounts to MyD88-dependent pulmonary
859 clearance of legionella pneumophila infection in vivo. *J Infect Dis*, *211*(2), 322-330.
860 https://doi.org/10.1093/infdis/jiu430
861 Matesanz, F., Potenciano, V., Fedetz, M., Ramos-Mozo, P., Abad-Grau Mdel, M., Karaky, M.,
862 Barrionuevo, C., Izquierdo, G., Ruiz-Pena, J. L., Garcia-Sanchez, M. I., Lucas, M., Fernandez,
863 O., Leyva, L., Otaegui, D., Munoz-Culla, M., Olascoaga, J., Vandenbroeck, K., Alloza, I.,

Astobiza, I., Antiguedad, A., Villar, L. M., Alvarez-Cermeno, J. C., Malhotra, S., Comabella, M., Montalban, X., Saiz, A., Blanco, Y., Arroyo, R., Varade, J., Urcelay, E., & Alcina, A. (2015). A functional variant that affects exon-skipping and protein expression of SP140 as genetic mechanism predisposing to multiple sclerosis. *Hum Mol Genet*, *24*(19), 5619-5627. https://doi.org/10.1093/hmg/ddv256

Mayer-Barber, K. D., Andrade, B. B., Oland, S. D., Amaral, E. P., Barber, D. L., Gonzales, J., Derrick, S. C., Shi, R., Kumar, N. P., Wei, W., Yuan, X., Zhang, G., Cai, Y., Babu, S., Catalfamo, M., Salazar, A. M., Via, L. E., Barry, C. E., 3rd, & Sher, A. (2014). Host-directed therapy of tuberculosis based on interleukin-1 and type I interferon crosstalk. *Nature*, *511*(7507), 99-103. https://doi.org/10.1038/nature13489

McNab, F., Mayer-Barber, K., Sher, A., Wack, A., & O'Garra, A. (2015). Type I interferons in infectious disease. *Nat Rev Immunol*, *15*(2), 87-103. https://doi.org/10.1038/nri3787

Mehta, S., Cronkite, D. A., Basavappa, M., Saunders, T. L., Adiliaghdam, F., Amatullah, H., Morrison, S. A., Pagan, J. D., Anthony, R. M., Tonnerre, P., Lauer, G. M., Lee, J. C., Digumarthi, S., Pantano, L., Ho Sui, S. J., Ji, F., Sadreyev, R., Zhou, C., Mullen, A. C., Kumar, V., Li, Y., Wijmenga, C., Xavier, R. J., Means, T. K., & Jeffrey, K. L. (2017). Maintenance of macrophage transcriptional programs and intestinal homeostasis by epigenetic reader SP140. *Sci Immunol*, *2*(9). https://doi.org/10.1126/sciimmunol.aag3160

Moreira-Teixeira, L., Mayer-Barber, K., Sher, A., & O'Garra, A. (2018). Type I interferons in tuberculosis: Foe and occasionally friend. *J Exp Med*, *215*(5), 1273-1285. https://doi.org/10.1084/jem.20180325

O'Connell, R. M., Saha, S. K., Vaidya, S. A., Bruhn, K. W., Miranda, G. A., Zarnegar, B., Perry, A. K., Nguyen, B. O., Lane, T. F., Taniguchi, T., Miller, J. F., & Cheng, G. (2004). Type I interferon production enhances susceptibility to Listeria monocytogenes infection. *J Exp Med*, *200*(4), 437-445. https://doi.org/10.1084/jem.20040712

Pan, H., Yan, B. S., Rojas, M., Shebzukhov, Y. V., Zhou, H., Kobzik, L., Higgins, D. E., Daly, M. J., Bloom, B. R., & Kramnik, I. (2005). Ipr1 gene mediates innate immunity to tuberculosis. *Nature*, *434*(7034), 767-772. https://doi.org/10.1038/nature03419

Perniola, R., & Musco, G. (2014). The biophysical and biochemical properties of the autoimmune regulator (AIRE) protein. *Biochim Biophys Acta*, *1842*(2), 326-337. https://doi.org/10.1016/j.bbadis.2013.11.020

Pichugin, A. V., Yan, B. S., Sloutsky, A., Kobzik, L., & Kramnik, I. (2009). Dominant role of the sst1 locus in pathogenesis of necrotizing lung granulomas during chronic tuberculosis infection and reactivation in genetically resistant hosts. *Am J Pathol*, *174*(6), 2190-2201. https://doi.org/10.2353/ajpath.2009.081075

Pilla-Moffett, D., Barber, M. F., Taylor, G. A., & Coers, J. (2016). Interferon-Inducible GTPases in Host Resistance, Inflammation and Disease. *J Mol Biol*, *428*(17), 3495-3513. https://doi.org/10.1016/j.jmb.2016.04.032

Pimentel, H., Bray, N. L., Puente, S., Melsted, P., & Pachter, L. (2017). Differential analysis of RNA-seq incorporating quantification uncertainty. *Nat Methods*, *14*(7), 687-690. https://doi.org/10.1038/nmeth.4324

Png, E., Alisjahbana, B., Sahiratmadja, E., Marzuki, S., Nelwan, R., Adnan, I., van de Vosse, E., Hibberd, M., van Crevel, R., Ottenhoff, T. H., & Seielstad, M. (2012). Polymorphisms in SP110 are not associated with pulmonary tuberculosis in Indonesians. *Infect Genet Evol*, *12*(6), 1319-1323. https://doi.org/10.1016/j.meegid.2012.04.006

909 Price, A., Caciula, A., Guo, C., Lee, B., Morrison, J., Rasmussen, A., Lipkin, W. I., & Jain, K.
910 (2019). DEvis: an R package for aggregation and visualization of differential expression data.
911 *BMC Bioinformatics*, *20*(1), 110. https://doi.org/10.1186/s12859-019-2702-z
912 Rayamajhi, M., Humann, J., Penheiter, K., Andreasen, K., & Lenz, L. L. (2010). Induction of
913 IFN-alphabeta enables Listeria monocytogenes to suppress macrophage activation by IFN-
914 gamma. *J Exp Med*, *207*(2), 327-337. https://doi.org/10.1084/jem.20091746
915 Roscioli, T., Cliffe, S. T., Bloch, D. B., Bell, C. G., Mullan, G., Taylor, P. J., Sarris, M., Wang,
916 J., Donald, J. A., Kirk, E. P., Ziegler, J. B., Salzer, U., McDonald, G. B., Wong, M., Lindeman,
917 R., & Buckley, M. F. (2006). Mutations in the gene encoding the PML nuclear body protein
918 Sp110 are associated with immunodeficiency and hepatic veno-occlusive disease. *Nat Genet*,
919 *38*(6), 620-622. https://doi.org/10.1038/ng1780
920 Scherer, M., & Stamminger, T. (2016). Emerging Role of PML Nuclear Bodies in Innate
921 Immune Signaling. *J Virol*, *90*(13), 5850-5854. https://doi.org/10.1128/JVI.01979-15
922 Schmidt, T., Schmid-Burgk, J. L., & Hornung, V. (2015). Synthesis of an arrayed sgRNA library
923 targeting the human genome OPEN. *Nature Publishing Group*, *5*, 14987-14987.
924 https://doi.org/10.1038/srep14987
925 Schneider, W. M., Chevillotte, M. D., & Rice, C. M. (2014). Interferon-stimulated genes: a
926 complex web of host defenses. *Annu Rev Immunol*, *32*, 513-545.
927 https://doi.org/10.1146/annurev-immunol-032713-120231
928 Shen, W., Le, S., Li, Y., & Hu, F. (2016). SeqKit: A Cross-Platform and Ultrafast Toolkit for
929 FASTA/Q File Manipulation. *PLOS ONE*, *11*(10), e0163962-e0163962.
930 https://doi.org/10.1371/journal.pone.0163962
931 Slager, S. L., Caporaso, N. E., de Sanjose, S., & Goldin, L. R. (2013). Genetic susceptibility to
932 chronic lymphocytic leukemia. *Semin Hematol*, *50*(4), 296-302.
933 https://doi.org/10.1053/j.seminhematol.2013.09.007
934 Stetson, D. B., & Medzhitov, R. (2006). Type I interferons in host defense. *Immunity*, *25*(3),
935 373-381. https://doi.org/10.1016/j.immuni.2006.08.007
936 Thye, T., Browne, E. N., Chinbuah, M. A., Gyapong, J., Osei, I., Owusu-Dabo, E., Niemann, S.,
937 Rusch-Gerdes, S., Horstmann, R. D., & Meyer, C. G. (2006). No associations of human
938 pulmonary tuberculosis with Sp110 variants. *J Med Genet*, *43*(7), e32.
939 https://doi.org/10.1136/jmg.2005.037960
940 Tosh, K., Campbell, S. J., Fielding, K., Sillah, J., Bah, B., Gustafson, P., Manneh, K., Lisse, I.,
941 Sirugo, G., Bennett, S., Aaby, P., McAdam, K., Bah-Sow, O., Lienhardt, C., Kramnik, I., &
942 Hill, A. V. S. (2006). Variants in the SP110 gene are associated with genetic susceptibility to
943 tuberculosis in West Africa. *Proc Natl Acad Sci U S A*, *103*(27), 10364-10368.
944 https://doi.org/10.1073/pnas.0603340103
945 Wang, H., Yang, H., Shivalila, C. S., Dawlaty, M. M., Cheng, A. W., Zhang, F., & Jaenisch, R.
946 (2013). One-step generation of mice carrying mutations in multiple genes by CRISPR/Cas-
947 mediated genome engineering. *Cell*, *153*(4), 910-918.
948 https://doi.org/10.1016/j.cell.2013.04.025
949 Weichenhan, D., Kunze, B., Winking, H., van Geel, M., Osoegawa, K., de Jong, P. J., & Traut,
950 W. (2001). Source and component genes of a 6-200 Mb gene cluster in the house mouse.
951 *Mamm Genome*, *12*(8), 590-594. https://doi.org/10.1007/s00335-001-3015-9
952 Zhang, S., Wang, X. B., Han, Y. D., Wang, C., Zhou, Y., & Zheng, F. (2017). Certain
953 Polymorphisms in SP110 Gene Confer Susceptibility to Tuberculosis: A Comprehensive

Review and Updated Meta-Analysis. *Yonsei Med J*, *58*(1), 165-173. https://doi.org/10.3349/ymj.2017.58.1.165

Zhu, A., Ibrahim, J. G., & Love, M. I. (2019). Heavy-tailed prior distributions for sequence count data: removing the noise and preserving large differences. *Bioinformatics*, *35*(12), 2084-2092. https://doi.org/10.1093/bioinformatics/bty895

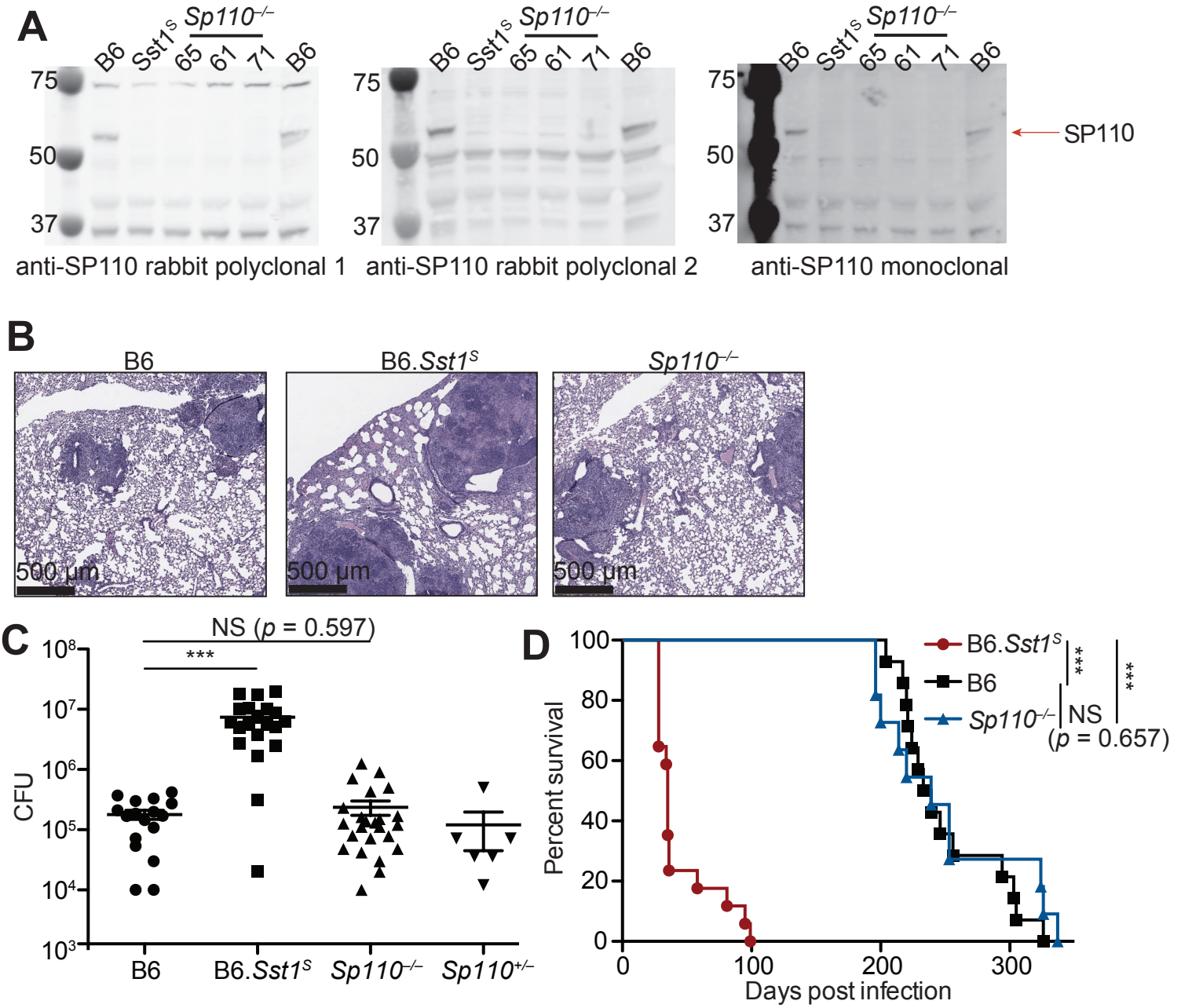

Figure 1. *Sp110*$^{-/-}$ mice are not susceptible to *M. tuberculosis* infections. (**A**) BMMs were treated with 10 U/ml of IFNγ for 24 hours and cells were lysed with RIPA buffer. Five µg of total protein was loaded on each lane, and immunoblot was performed with respective antibodies as shown. Molecular weight standards are shown on the left of each blot in kDa. Individual membranes were imaged separately. Three independent lines of *Sp110*$^{-/-}$ mice were analyzed (denoted lines 61, 65, and 71). (**B-D**)**,** Lungs of mice infected with *M. tuberculosis* were stained with hematoxylin and eosin (H&E) for histology (**B**)**,** measured for CFU at 25 days post-infection (Mann-Whitney test) (**C**) or, monitored for survival (**D**). All except B6 mice were bred in-house, and combined results from the three independent *Sp110*$^{-/-}$ lines are shown. Representative of 2 experiments (**B, D**); combined results of 3 infections (**C**). *, $p \leq 0.05$; **, $p \leq 0.01$; ***, $p \leq 0.005$.

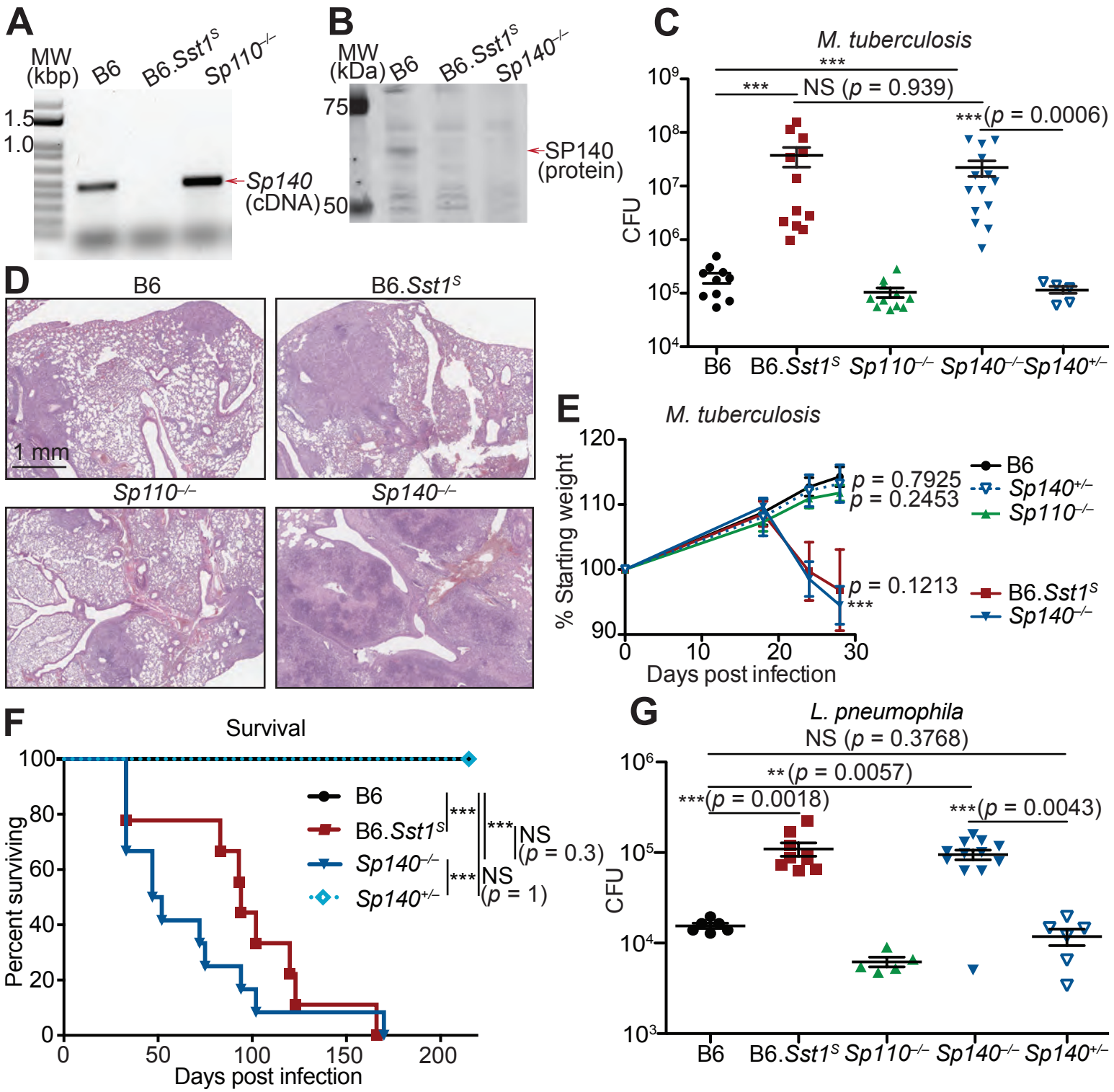

Figure 2. *Sp140*$^{-/-}$ mice are susceptible to bacterial pathogens. (**A**) RT-PCR of cDNA from BMMs of the indicated genotypes. Red arrow indicates band corresponding to a portion of Sp140, verified by sequencing. (**B**) Immunoblot of lysates from *Sp140*$^{-/-}$ and WT BMMs treated with 10 U/ml of recombinant mouse IFNγ for 24 hours. Equal amounts of protein were loaded for immunoblot with anti-SP140 antibody. (**C**-**F**) Mice were infected with *M. tuberculosis* and measured for (**C**) lung CFU at 28 days post-infection, (**E**) body weight over time, and (**F**) survival. Statistics in (**E**) shows comparison to B6 at day 28, and data are from 10 B6, 11 B6.*Sst1*^{S}, 11 *Sp110*$^{-/-}$, 14 *Sp140*$^{-/-}$, and 6 *Sp140*$^{+/-}$ mice. (**D**) H&E staining of lungs at 25 days post-infection with *M. tuberculosis*. Full histology images are provided in Figure 2 – figure supplement 2. (**G**) Mice were infected with *L. pneumophila* and lung CFUs were determined at 96 hours post-infection. All mice were bred in-house, *Sp140*$^{-/-}$ and *Sp140*$^{+/-}$ were littermates (**C**-**F**). **C**, **E**, and **G** are combined results of two independent infections. **A**-**D** shows representative analysis of one *Sp140*$^{-/-}$ line (line 1), whereas **F**-**G** includes a mixture of both lines 1 and 2. Results of infection of both lines with *M. tuberculosis* is shown in Figure 2 – figure supplement 1E. (**C**, **E**, **F**, **G**) Mann-Whitney test. *, $p \leq 0.05$; **, $p \leq 0.01$; ***, $p \leq 0.005$.

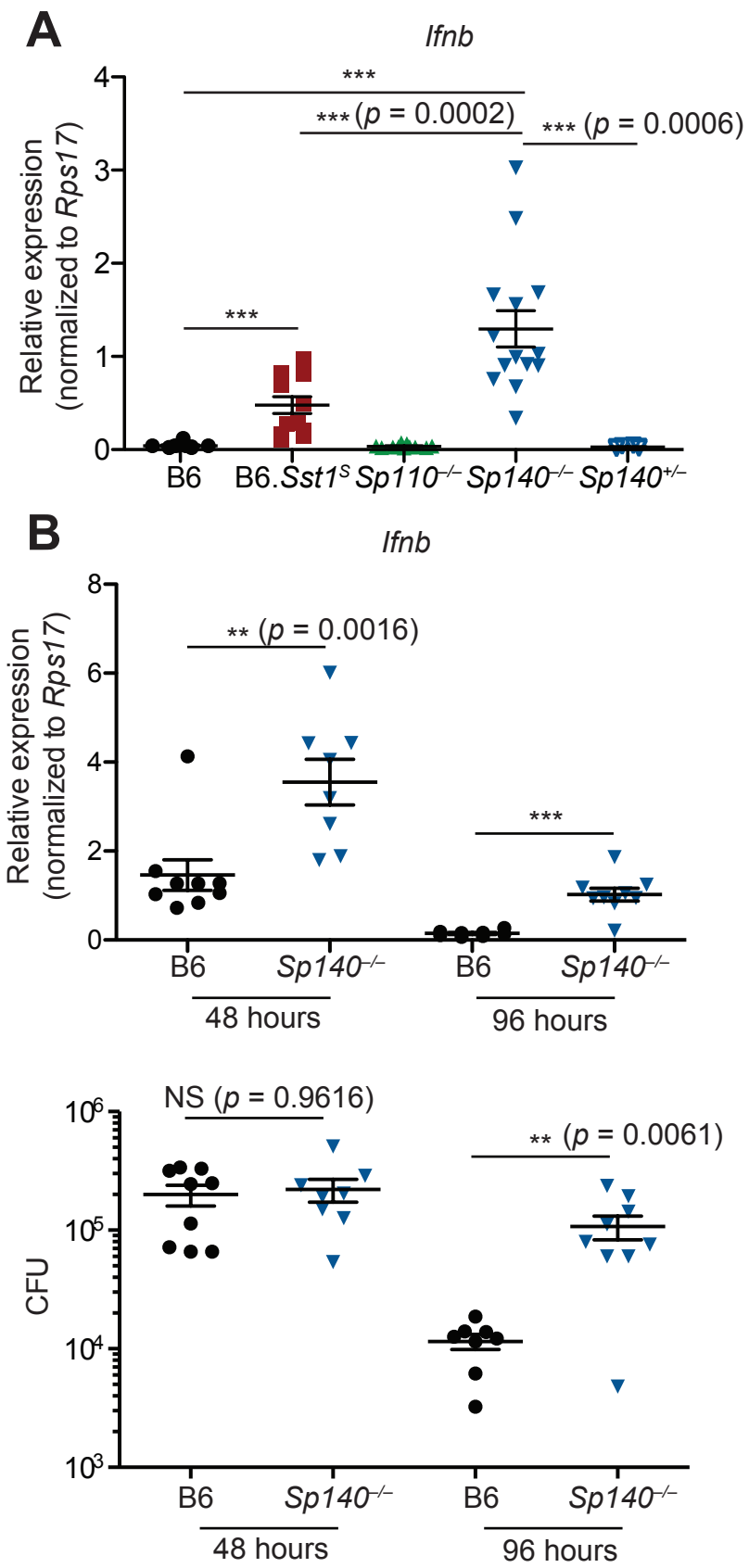

Figure 3. *Sp140*$^{-/-}$ mice have elevated *Ifnb* transcripts during bacterial infection. (**A**) Mice were infected with *M. tuberculosis* and at 28 days post-infection lungs were processed for total RNA, which was used for RT-qPCR. Combined results of 2 independent experiments. (**B**) Mice were infected with *L. pneumophila* and RT-qPCR (top panel) and CFU enumeration (bottom panel) was performed on lungs collected at indicated times. Combined results of 2 independent infections. All mice were bred in-house, *Sp140*$^{-/-}$ and *Sp140*$^{+/-}$ were littermates. (**A**-**B**) Mann-Whitney test. *, $p \leq 0.05$; **, $p \leq 0.01$; ***, $p \leq 0.005$.

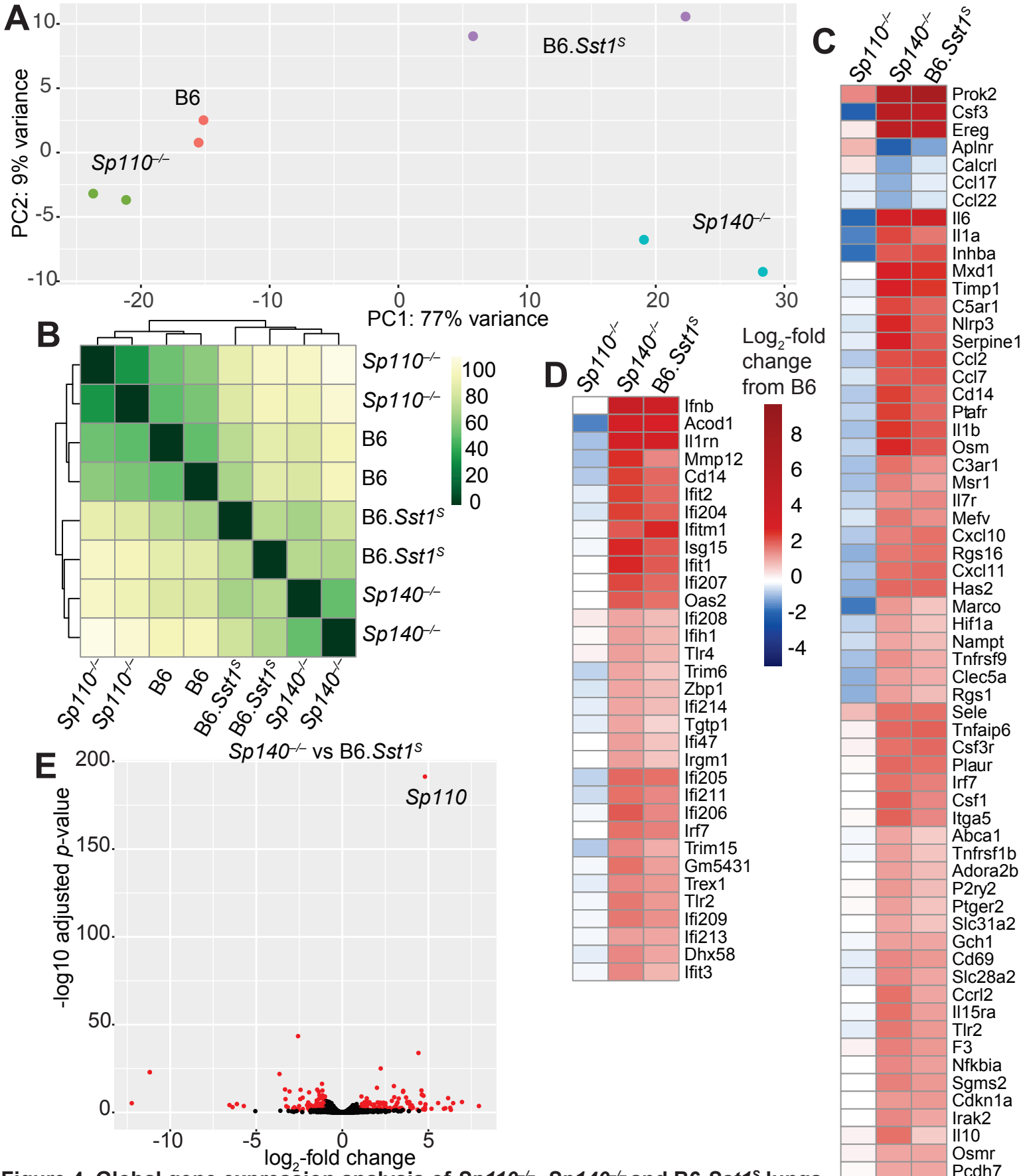

Figure 4. Global gene expression analysis of *Sp110*$^{-/-}$, *Sp140*$^{-/-}$ and B6.*Sst1*^{S} lungs after *M. tuberculosis* infection. (**A**) PCA or (**B**) Euclidean distance analysis of all the samples. (**C**-**D**) Heatmaps of gene expression in $\log_2$-fold change from *M. tuberculosis*-infected B6. Genes shown are those significantly different between *Sp140*$^{-/-}$ and B6: (**C**) GSEA Hallmark inflammatory response; and (**D**) GO type I IFN response genes. (**E**) Volcano plot comparing *Sp140*$^{-/-}$ to B6.*Sst1*^{S} expression. Dots in red are 2-fold differentially expressed with adjusted *p*-value ≤ 0.05.

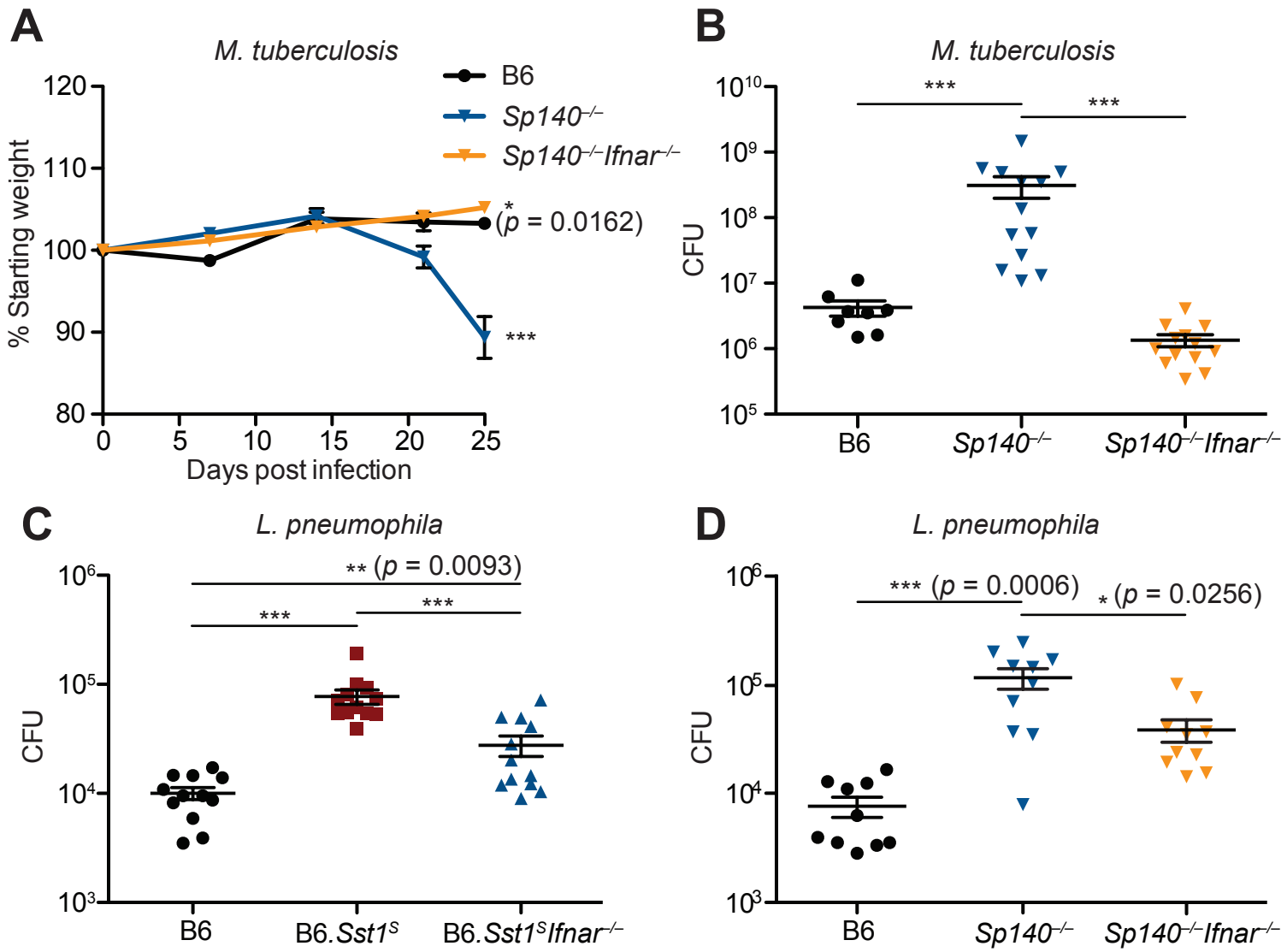

Figure 5. Susceptibility of *Sp140*$^{-/-}$ to *M. tuberculosis* and *L. pneumophila* is dependent on type I IFN signaling. (**A**-**B**) mice were infected with *M. tuberculosis* and measured for (**A**) body weight, and (**B**) bacterial burdens at day 25. Statistics in **A** show comparison to B6; data are from 9 B6, 13 *Sp140*$^{-/-}$, and *Sp140*$^{-/-}$ *Ifnar*$^{-/-}$ mice. Combined results of 2 experiments. (**C**-**D**) bacteria burden in *L. pneumophila*-infected mice at 96 hours. Combined results of 2 experiments. All mice were bred in-house (**A**-**B**, **D**); all but B6 were bred in-house (**C**). Mann-Whitney test (**A**-**D**). *, $p \leq 0.05$; **, $p \leq 0.01$; ***, $p \leq 0.005$.

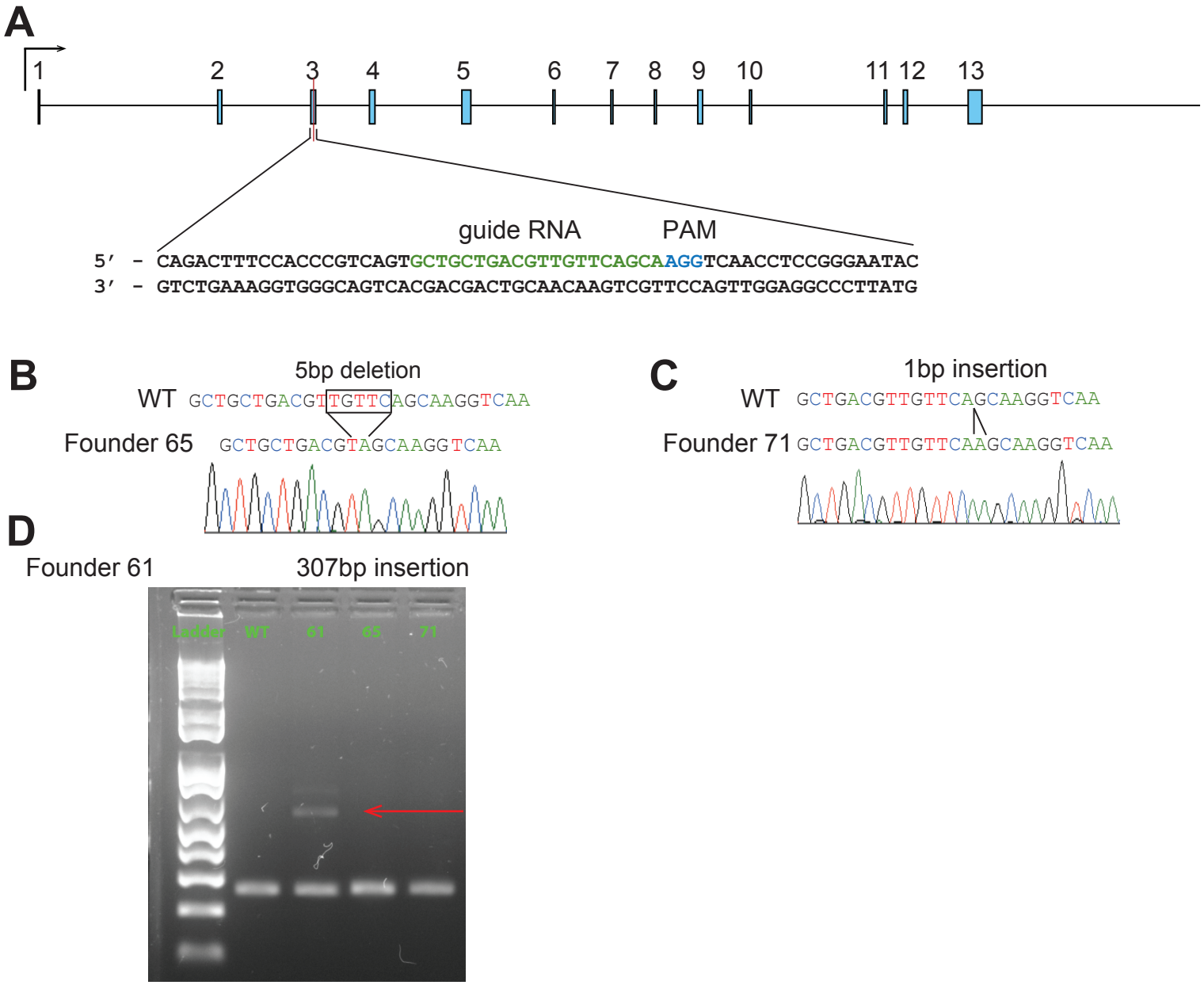

Figure 1 – figure supplement 1. CRISPR–Cas9 targeting strategy for *Sp110*$^{-/-}$ mice. (**A**) Mouse *Sp110* gene. Guide RNA sequence for CRISPR–Cas9 targeting and protospacer-adjacent motif (PAM) are indicated. (**B**-**D**) *Sp110* locus in wildtype (WT) and three independent lines. Homozygotes of 2 lines identified by sequencing (**B**-**C**), and heterozygote of the 3rd line by PCR products separated on an agarose gel (**D**). Arrow indicates the mutant band.

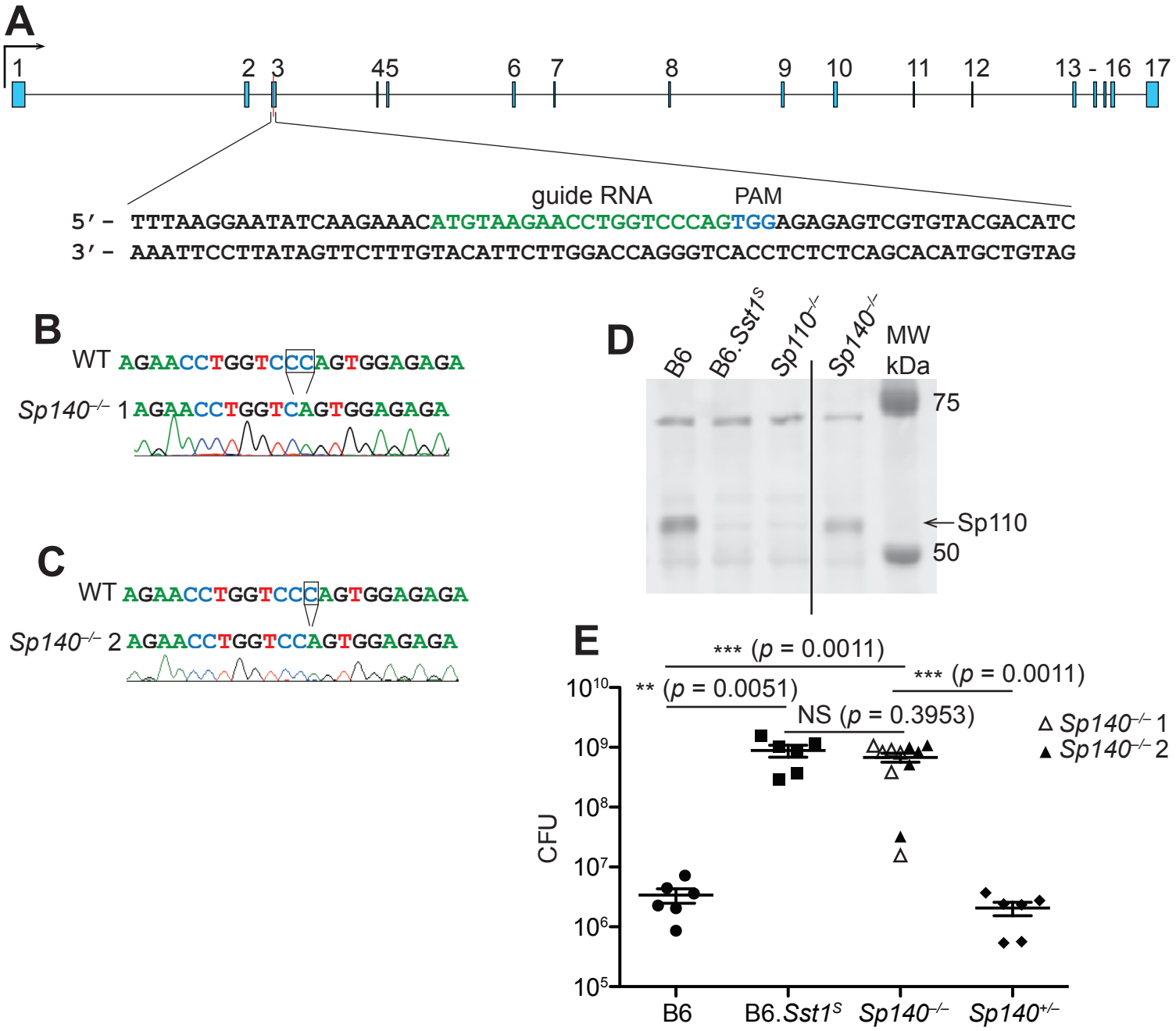

Figure 2 – figure supplement 1. CRISPR–Cas9 targeting strategy for *Sp140*$^{-/-}$ and validation of founders. (**A**) Mouse *Sp140* gene. Guide RNA sequence for CRISPR–Cas9 targeting and protospacer-adjacent motif (PAM) are indicated. (**B**-**C**) *Sp140* locus in wildtype (WT) and 2 independent founders of *Sp140*$^{-/-}$ validated by sequencing. (**D**) Immunoblot for SP110 using BMMs from mice of the indicated genotypes. Intervening lanes have been removed for clarity (indicated by line in the image). (**E**) *M. tuberculosis*-infected mice were harvested for CFU at 25 days post-infection. Empty and filled triangles indicate the two independent lines of *Sp140*$^{-/-}$ used in this infection. All mice were bred in-house and *Sp140*$^{+/-}$ were littermates with *Sp140*$^{-/-}$ line 2. Mann-Whitney test, *, $p \leq 0.05$; **, $p \leq 0.01$; ***, $p \leq 0.005$.

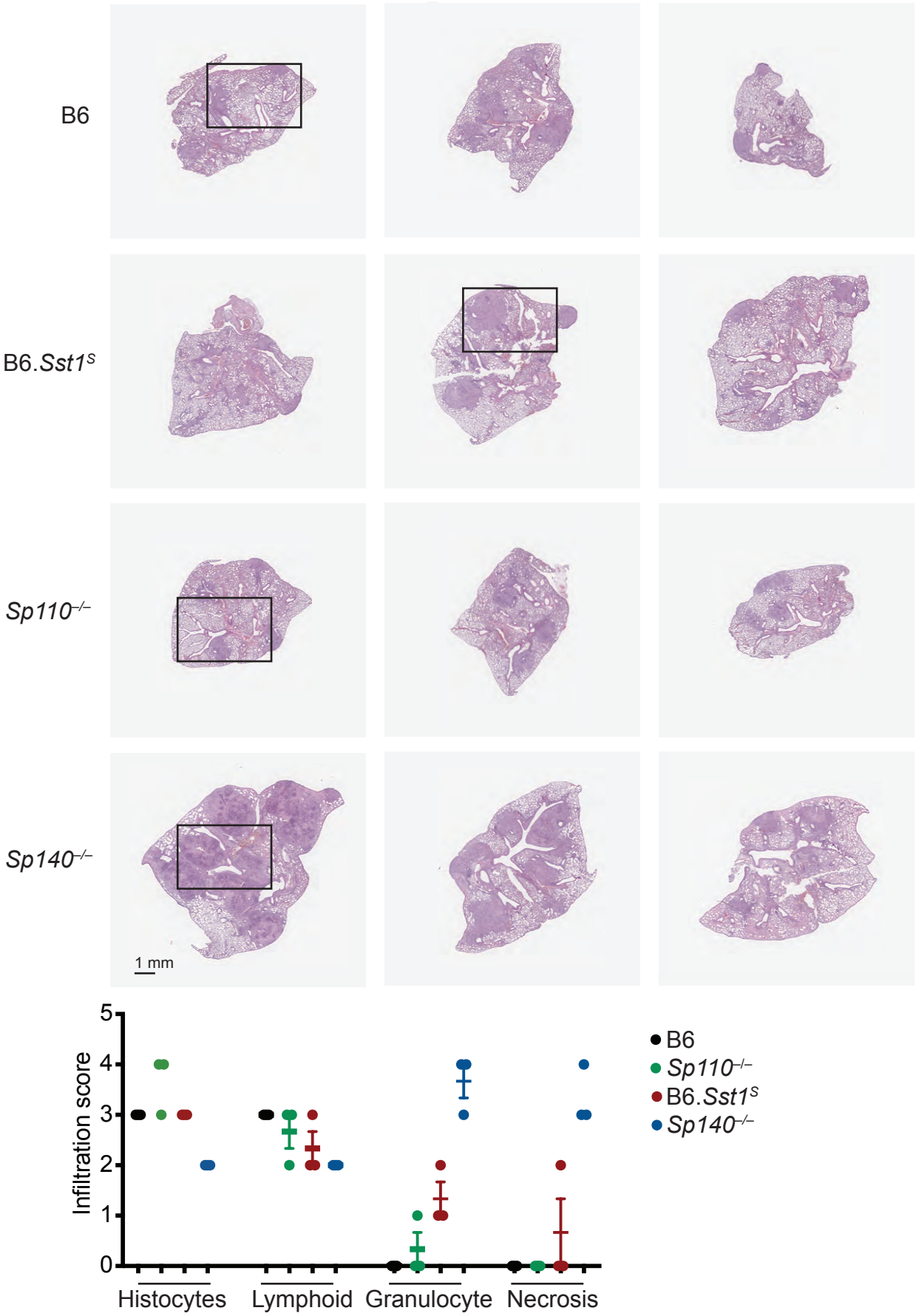

Figure 2 – figure supplement 2. Histology of lungs from B6, B6.*Sst1*^{S}, *Sp110*$^{-/-}$, *Sp140*$^{-/-}$ mice after infection with *M. tuberculosis*. H&E staining of entire lung sections from mice of indicated genotypes at 25 days post-infection with *M. tuberculosis*. Black squares denote sections shown in Figure 2C. Each image represents a lung section from a different mouse. Borders in background color have been added around each image. Scale bar applies to all images. Samples were evaluated and scored (0-4, least to most) for macrophage (histocyte), lymphoid, granulocyte infiltration, and extent of necrosis.

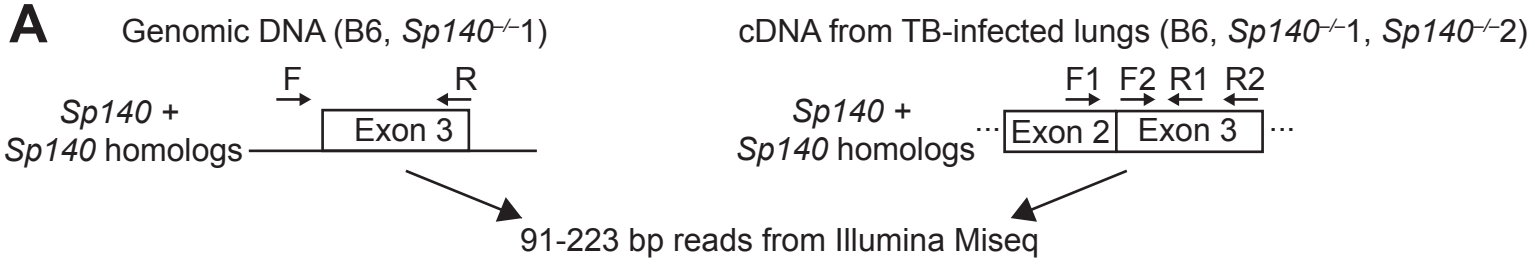

B

Summary of edited *Sp140* homologs in *Sp140*$^{-/-}$ mice

Name	Dataset	Distinguishing SNPs from *Sp140* mRNA	Edited in *Sp140*$^{-/-}$*1?*	Edited in *Sp140*$^{-/-}$*2?*	Estimated level of expression in TB-infected lungs
LOC100041057	*Sp140* exon 3 amplicons, DNA (*Sp140*$^{-/-}$1 and B6)	G at 1483, T at 1513	Yes	Unknown (not expressed)	None
Sp140 homolog 1	*Sp140* exon 3 amplicons, DNA (*Sp140*$^{-/-}$1 and B6)	T at 1482, G at 1483	Yes	Unknown (not expressed)	None
Sp140 homolog 2	*Sp140* exon 2, 3 amplicons, cDNA; RNA-seq of TB-infected lungs	None	Yes	No	Expressed
Sp140 homolog 3	*Sp140* exon 3 amplicons, cDNA	T at 1462	Yes	Yes	Very low (not detectable by RNA-seq)
Sp140 homolog 4	*Sp140* exon 3 amplicons, cDNA	T at 1500	Yes	Yes	Very low (not detectable by RNA-seq)

Figure 2 – figure supplement 3. Characterization of off-target genes mutated in *Sp140*$^{-/-}$ mice. (**A**) Schematic of amplicon sequencing strategy for *Sp140* and *Sp140* homologs. (**B**) Summary of edited *Sp140* homologs from amplicon sequencing and RNA-seq analysis. SNPs are denoted based on the *Sp140* X1 transcript. Expression level was roughly estimated from read counts. Three B6 and 2 *Sp140*$^{-/-}$ mice from each founder line were used as biological replicates for *Sp140* exon 2/3 amplicon sequencing from cDNA, 2 mice per genotype were used for *Sp140* exon 3 amplicon sequencing from cDNA, and 1 mouse per genotype was used for *Sp140* exon 3 amplicon sequencing from DNA.

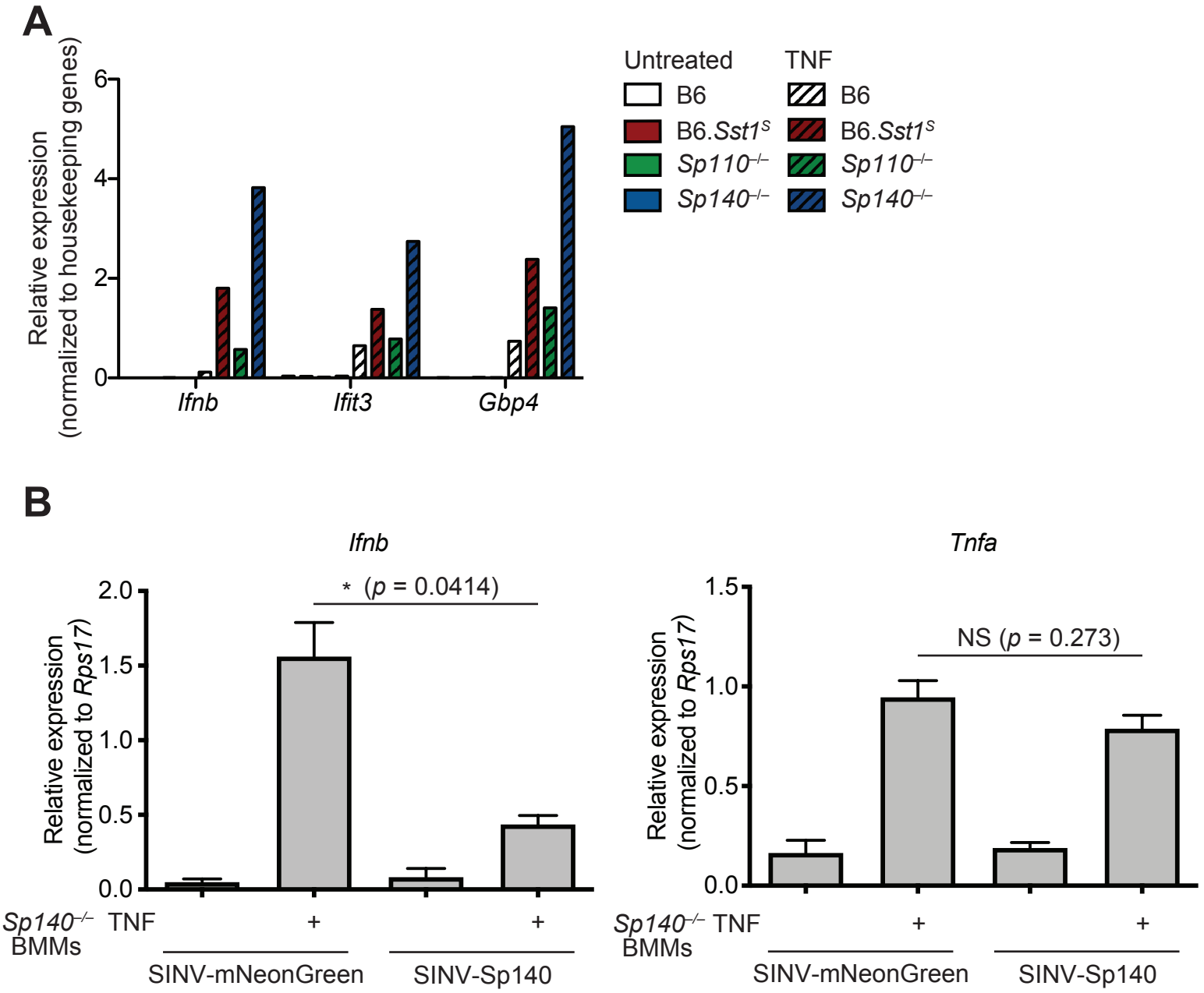

Figure 2 – figure supplement 4. Complementation of hyper type I IFN responses in *Sp140*$^{-/-}$ BMMs. (**A**) BMMs were left untreated or treated with TNF-α for 24 hours. Total RNA was used for RT-qPCR. Averages of technical duplicates for one biological replicate are shown. Data is representative of two independent experiments. (**B**) RT-qPCR of *Sp140*$^{-/-}$ BMMs transduced with either control SINV-minCMV-GAL4-mNeonGreen (SINV-mNeonGreen) or SINV-minCMV-Sp140 (SINV-Sp140), primed with 5 ng/mL IFN-γ for 14 hours and treated with 10 ng/mL TNF-α for 4 hours. *, $p \leq 0.05$ calculated with an unpaired t-test with Welch's correction. Data are representative of two independent experiments.

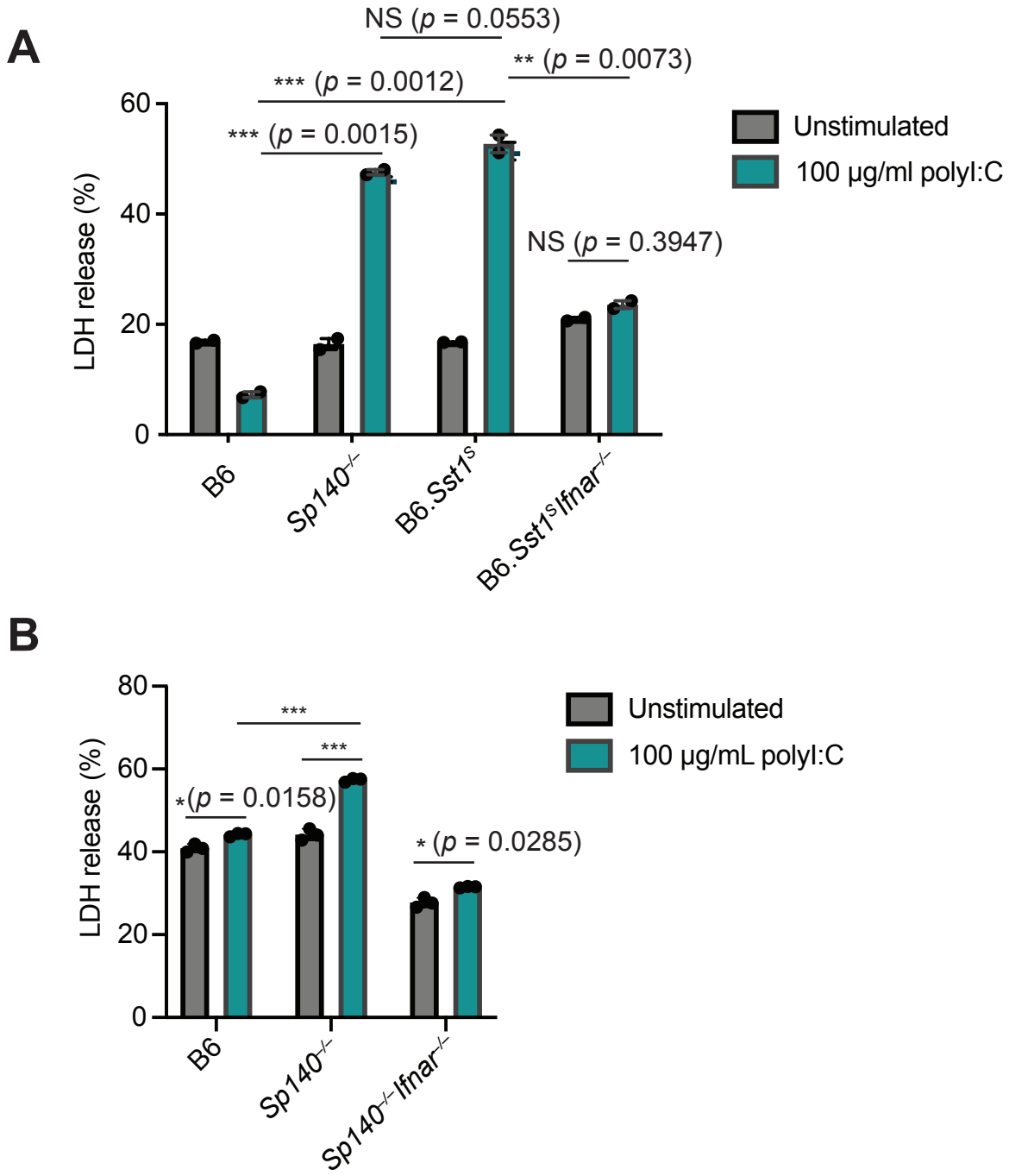

Figure 3 – figure supplement 1. BMMs from B6.*Sst1*^{S} and *Sp140*$^{-/-}$ mice show increased cell death upon stimulation with polyI:C, which is dependent upon IFNAR signaling. LDH release from primary BMMs after 16-24 hour stimulation with 100 µg/mL polyI:C for (**A**) B6, B6.*Sst1*^{S}, *Sp140*$^{-/-}$, B6.*Sst1*^{S}*Ifnar*$^{-/-}$ mice. Results are technical duplicates and representative of three independent experiments for B6 (3 mice), B6.*Sst1*^{S} (2 mice), and *Sp140*$^{-/-}$ (2 mice) samples, and two independent experiments for B6.*Sst1*^{S}*Ifnar*$^{-/-}$ sample (1 mouse). (**B**) LDH release after polyI:C stimulation for primary BMMs from B6, *Sp140*$^{-/-}$, and *Sp140*$^{-/-}$*Ifnar*$^{-/-}$ mice. Results represent technical triplicates and are representative of two independent experiments for two mice per genotype. *, $p \leq 0.05$; **, $p \leq 0.01$; ***, $p \leq 0.005$ as calculated with an unpaired t-test with Welch's correction.

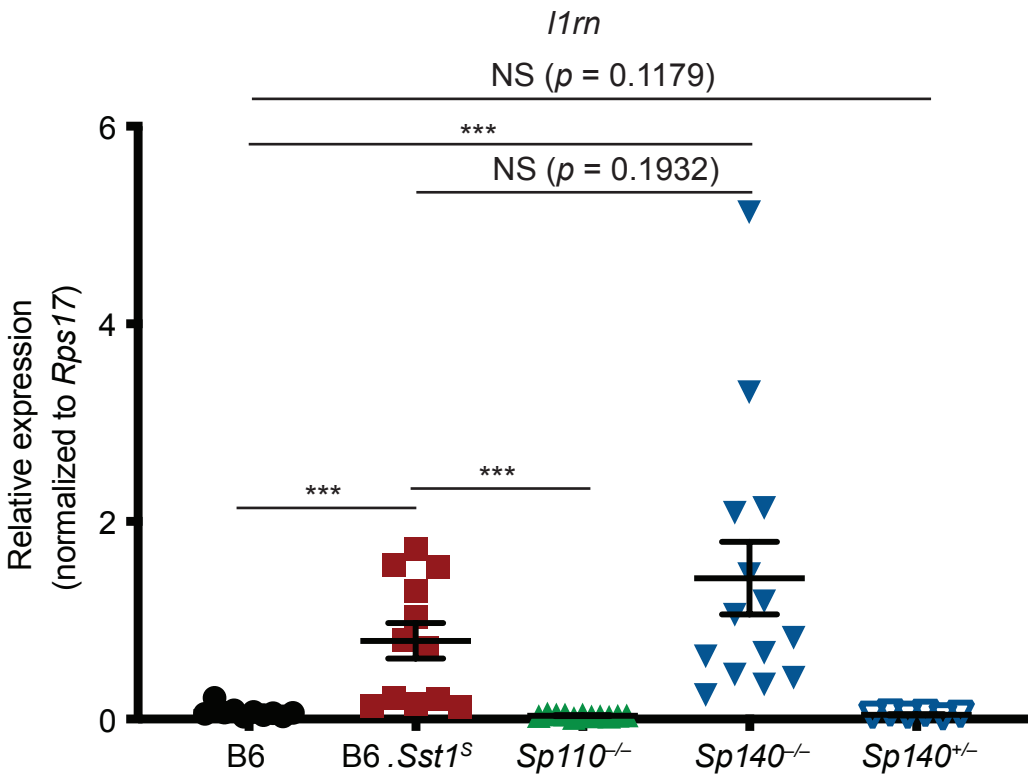

Figure 4 – figure supplement 1. B6.*Sst1*^{S} and *Sp140*$^{-/-}$ lungs exhibit elevated transcript levels of the interferon stimulated gene Il1rn during *M. tuberculosis* infection. RT-qPCR for *Il1rn* (encodes Il1ra) for RNA extracted from lungs at 28 days post-infection with *M. tuberculosis*. Combined results of two independent experiments. Mann-Whitney test, *, $p \leq 0.05$; **, $p \leq 0.01$; ***, $p \leq 0.005$.

	***Sp110*$^{-/-}$ vs. B6**		***Sp140*$^{-/-}$ vs. B6**		***Sp110*$^{-/-}$ vs. B6.*Sst1*^{S}**		***Sp140*$^{-/-}$ vs. B6.*Sst1*^{S}**	
Gene	**Log2-fold change**	**Adjusted *p*-value**	**Log2-fold change**	**Adjusted *p*-value**	**Log2-fold change**	**Adjusted *p*-value**	**Log2-fold change**	**Adjusted *p*-value**
Sp100	-0.1578	0.2936	0.3825	0.0088	-0.3877	0.0578	0.1123	0.5792
Sp110	-0.7750	1.4E-12	0.3382	0.0025	3.2647	1.00E-52	4.4200	4.26E-97
Sp140	-0.4293	0.0343	-0.4480	0.0303	1.7591	1.49E-14	1.7976	3.64E-14

Figure 4 – figure supplement 2. Expression of SP family members in *Sp140*$^{-/-}$ and *Sp110*$^{-/-}$ mouse lungs during *M. tuberculosis* infection. Log_2-fold change and adjusted *p*-value for SP family members (*Sp100*, *Sp110*, *Sp140)* from RNA-seq of *M. tuberculosis*-infected lungs from *Sp110*$^{-/-}$ and *Sp140*$^{-/-}$ mice, compared to B6 and B6.*Sst1*^{S}.

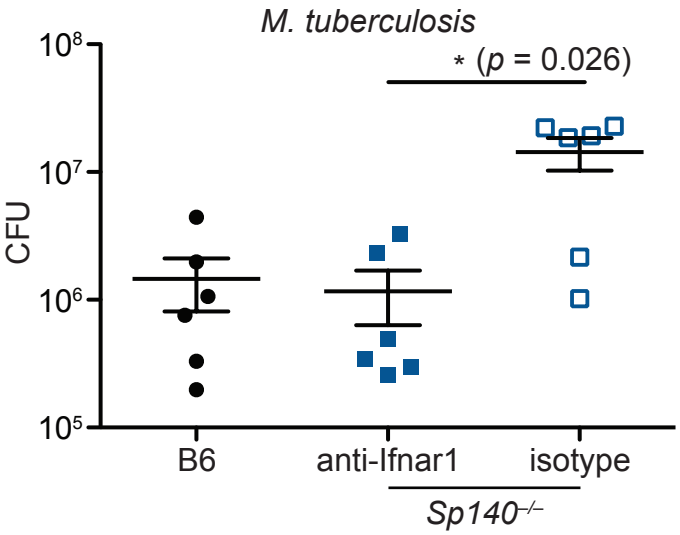

Figure 5 – figure supplement 1. Antibody blockade of IFNAR1 reduces bacterial burden in *Sp140*$^{-/-}$ mice during *M. tuberculosis* infection. Mice were infected with *M. tuberculosis* and treated with either IFNAR1-blocking antibody or isotype control starting 7 days post-infection. At 25 days post-infection lungs were harvested to enumerate CFU. Results of one experiment. All mice were bred in-house. Mann-Whitney test, *, $p \leq 0.05$; **, $p \leq 0.01$; ***, $p \leq 0.005$.